

Mechanisms for concentrating critical metals in granitic complexes: insights from the Mourne Mountains, Northern Ireland




K. R. Moore^{1*}, N. R. Moles², G. K. Rollinson¹ and P. A. J. Lusty³

¹ Camborne School of Mines, University of Exeter, Penryn Campus, Treliver Road, Penryn, Cornwall TR10 9FE, UK

² School of Applied Sciences, University of Brighton, Cockcroft Building, Lewes Road, Brighton BN2 4GJ, UK

³ British Geological Survey, Environmental Science Centre, Nicker Hill, Keyworth, Nottingham NG12 5GG, UK

 KRM, 0000-0003-0182-3204; NRM, 0000-0003-1399-9709; GKR, 0000-0002-0655-6304; PAJL, 0009-0000-3393-0237

* Correspondence: k.moore@exeter.ac.uk

Abstract: The Tellus stream sediment and deep soil geochemistry data sets for Northern Ireland were used to locate four types of critical metals anomalies in granite bedrocks of the Mourne Mountains. A curvi-linear array of Nb, REE, Th and U soil anomalies across the eastern Mourne Mountains correlated with late-stage and eutectic temperature minerals in the roof zone of the most peralkaline F- and volatile-rich granite body, remobilized on micron to millimetre scales. Li, Be, B, As, Sn, Mn³⁺ and Ce⁴⁺ partitioned into pockets of late-stage heterogeneously distributed F-rich silicic residual melts and relatively oxidizing halide-rich magmatic fluids, resulting in drusy mineral and hydrothermal assemblages. Isolated soil anomalies correlated with amorphous Mn³⁺- and Ce⁴⁺-rich masses infilling drusy cavities, which resulted from short-distance percolation of small volumes of late-stage magmatic fluids. A significant As plume in stream sediments emanated from a greisen that hosted multiple critical and base metals including Sn, from reactions between large volumes of magmatic As + halide-rich fluids and mafic silicate + diverse accessory minerals on the metre- to kilometre-scale along geological structures. Diverse, small-scale REE anomalies in the soil data along structural features in the western Mournes correlate with vein mineralization resulting from episodic migration of hydrous fluids of variable composition, probably with a much smaller magmatic component than elsewhere. The regional geochemical dataset proved useful to develop a multi-stage model for enrichment of critical metals in the Mourne Mountains granites, which is analogous to the petrogenesis of some of the igneous-hosted economic deposits of critical metals.

Thematic collection: This article is part of The energy-critical metals for a low carbon transition collection available at: <https://www.lyellcollection.org/topic/collections/critical-metals>

Received 20 July 2023; revised 7 November 2023; accepted 4 December 2023

The description of a metal or semi-metal as a critical raw material (CRM) depends on the perspective of the end-user and the degree of ‘criticality’ as calculated using complex multi-dimensional methodologies (Graedel *et al.* 2012, 2014, 2015; Chakhmouradian *et al.* 2015; Hayes and McCullough 2018). The European Commission published five lists of CRMs between 2011 and 2023 (European Commission 2023) and the UK has an independent list of CRMs (BGS 2022). The term ‘critical metal’ is now widely applied to geologically-available metals with specialist chemical and physical properties that are used in small but increasing quantities in the manufacture of new technologies, which may be subject to supply restrictions (Moss *et al.* 2011; Reck and Graedel 2012; Graedel *et al.* 2014; Lusty and Gunn 2014). Potential supply shortages cannot be fully offset by increased recycling rates due to dispersion of critical metals in technological devices, longevity of use of some of the technological devices, manufacturing design and alloying with metals that increase the difficulty of separation, and lack of effective substitute metals (Steinbach and Wellmer 2010; Du and Graedel 2011; Binnemans *et al.* 2013; Bloodworth 2014; Graedel *et al.* 2015; Hagelüken and Goldmann 2022). Supply security for European manufacturing could be increased by better understanding of the occurrence of critical metal ore deposits in Europe and their potential for development (Moss *et al.* 2011; Bertrand *et al.* 2016; Goodenough *et al.* 2016). However, there is less information on the occurrence and concentration of critical metals than for metals that are used in large quantities (Graedel *et al.* 2014). The research presented here describes and interprets the mineral and chemical characteristics of localities in a granite complex where

critical metals, such as rare earth elements (REE) and Nb, are concentrated above background levels.

A new opportunity to investigate the occurrence of critical metal in a geological terrane in Europe is afforded by the Tellus project (Lusty 2016; Moore *et al.* 2016). The aims of the Tellus project were to generate the geological information to plan and manage sustainable development of Northern Ireland’s natural resources, and to measure and assess the environmental well-being of the region (Smyth 2007; Earls 2016; Young 2016). Between 2004 and 2013 the project comprised a programme of detailed mapping of rocks, soils and water by geophysical and geochemical methods (Smyth 2007; Cooper *et al.* 2012; Hodgson and Young 2016; Young *et al.* 2016). The Mourne Mountains in County Down, Northern Ireland, were surveyed during the Tellus NI project of 2004–07 (Moore *et al.* 2016; Young *et al.* 2016), and they were historically (largely over the last 40 years) explored for a wide range of metals, particularly U, Au, base metals (Cu, Zn, Pb), Sn, Ta and Nb. Cassiterite has been reported from across the area in a variety of geological environments (Seymour 1903; Arthurs and Earls 2004; Warner *et al.* 2010; Moles *et al.* 2013) and REE, Nb and Ta are present in granites and alluvial heavy mineral concentrates (Moles and Higgins 1995; Moles and Tindle 2011; MacDonald *et al.* 2013; Goodenough *et al.* 2016; Moore *et al.* 2016). REE-minerals (e.g. fergusonite and gadolinite) in soil and stream sediments of the Mourne Mountains show little evidence of breakdown (Moles and Tindle 2011) but the occurrence of secondary U minerals on joint faces in the granites and soils (Moles and Higgins 1995; McAlister *et al.* 1997; Arthurs and Earls 2004) raises significant questions over

whether U is coupled to REE enrichments. There have been no detailed investigations of the REE, their distribution and their coupling to Nb, Ta and other critical metals, despite the occurrence of a variety of critical metal-bearing minerals in the granites (e.g. fergusonite, gadolinite, bismutite, russellite; Moles and Tindle 2011, 2012) and inclusion of the Mourne Mountains granites in a review of potential geological resources for critical metals in Europe (Goodenough *et al.* 2016).

The importance of detailed mineralogical analysis to develop petrogenetic models that define vectors towards rocks that host enrichments of critical metals in mineral systems models (Banks *et al.* 2019, 2020; Steiner 2019) drove the ethos of the investigation. The aims of this research are: (1) to use the Tellus data to identify where critical metals, radioactive elements and other potential commodities are more concentrated than background concentrations in the Mourne Mountains granites; (2) to elucidate as far as possible the magmatic \pm hydrothermal processes that concentrated metals in the bedrock at these sites; (3) to place these processes in the context of the established petrogenetic models for granite formation, as described in the Geological Setting below. While the geological processes under investigation relate to exploration for ore deposits, we do not suggest that any critical metal enrichment in the Mourne Mountains will be of economic value since we have not determined the recovery, spatial distribution or the abundance of critical metals from mineral hosts by mineral processing techniques. A detailed examination of alluvial sediments and heavy mineral concentrates formed part of the research and is alluded to in this manuscript, but the detailed results are currently unpublished.

Geological setting

The British–Irish Paleogene Igneous Province (BIPIP) is a large igneous province, stretching from Greenland to the British Isles, that comprises flood-basalts with associated intrusive rocks that were emplaced before and during North Atlantic sea-floor spreading (Kent and Fitton 2000; Stuart *et al.* 2000; Storey *et al.* 2007; Hansen *et al.* 2009; Hole and Millett 2016; Wilkinson *et al.* 2017). The BIPIP has been chemically linked to an ancestral Icelandic mantle plume. Radiogenic and stable isotopic investigations conclude that the BIPIP is dominated by a heterogeneous mantle signature with greatest contamination by crustal sources and meteoric fluids in the centres of magmatism in western Scotland (O'Connor 1988; Meighan *et al.* 1992; Stuart *et al.* 2000; Jolley and Bell 2002; Hughes *et al.* 2015). The late stages of magmatic activity included intrusive granites, central complex magmatism and acidic extrusive rocks (Walker 1975; Gibson *et al.* 1987; Thompson *et al.* 1987; Gamble *et al.* 1999; Ganerød *et al.* 2011).

A continuum of lithological compositions have been interpreted on the basis of chemical studies and used to suggest a model of extensive fractionation to generate granitic magma compositions from parental basaltic magmas (Meighan and Gamble 1972; Tammemagi 1976; Meighan *et al.* 1984). The multiple intrusive centres in the BIPIP include the granites in St. Kilda, Arran, Skye and the Mourne Mountains, from where chevkinite-group minerals, fergusonite, gadolinite, allanite, monazite and zirkelite have been reported (Harding *et al.* 1982; Hyslop *et al.* 1999; Moles and Tindle 2011; MacDonald *et al.* 2013; Goodenough *et al.* 2016).

The Mourne Mountains Complex intrudes Lower Paleozoic metasediments of the Southern Uplands-Down-Longford Terrane and cuts across a Tertiary dyke swarm, though the granites are subsequently intruded by a small number of dykes (Walker 1975; Meighan *et al.* 1988; Gamble *et al.* 1999). The complex comprises five granite intrusions in two distinct centres (Fig. 1a), three granites (G1–G3) in the eastern centre and two granites (G4–G5) in the contiguous western centre (Richey 1928; Emeleus 1955; Hood

1981; Gibson 1984; Meighan *et al.* 1984; Stevenson *et al.* 2007; Stevenson and Bennett 2011). The intrusions in each of the two centres young from the east to the west, although the radiometric ages of all the granites cluster around 56 Ma (Gibson *et al.* 1987, 2003; Gamble *et al.* 1999). The Mourne Mountains Complex was emplaced *c.* 6 Ma after the onset of basaltic magmatism in Antrim (Northern Ireland) and Greenland (Ganerød *et al.* 2011; Wilkinson *et al.* 2017).

The petrography and geochemistry of the granites has been described previously (Hood 1981; Gibson 1984; Meighan *et al.* 1984, 1988). G1 is a calcic amphibole-biotite (\pm fayalite) granite with the lowest bulk silica content of the complex: it is the least fractionated of the granites and has a subalkaline composition. G2, G3 and G4 are biotite granites that are metaluminous to peraluminous, where G2 contains a variable mafic content and G4 contains muscovite. G5 is a calcic amphibole-biotite granite with bulk silica concentration comparable to G2, G3 and G4 granite. Granites of both the eastern and western Mourne Mountains contain miarolitic cavities and greisens have also been reported from the eastern Mourne (Nockolds and Richey 1939; McCormick *et al.* 1993; Moore *et al.* 2016). High Rb, low Sr and large Eu anomalies demonstrate the highly fractionated nature of the granites (Meighan *et al.* 1984). However, significant differences between initial $^{87}\text{Sr}/^{86}\text{Sr}$ ratios suggests that a simple fractionation relationship cannot entirely explain the relationship between the granites and that there was more than one magmatic pulse (Meighan *et al.* 1988; Gibson *et al.* 2003). $\delta^{18}\text{O}$ data illustrates that circulation of meteoric water significantly affected host rocks and intrusions outside the granite, but had only a minor and localized effect on the granites, close to the margins of the plutons, near internal contacts or near greisens (Meighan *et al.* 1992; McCormick *et al.* 1993). δD was higher in samples that had evidence of chloritization as a consequence of autometamorphism by exsolved magmatic fluids (McCormick *et al.* 1993).

The first model for emplacement of the Mourne Mountains Granite Complex involved cauldron subsidence (Richey 1928) but recent studies using the anisotropy of magnetic susceptibility favour an emplacement model of laccolith inflation (Stevenson *et al.* 2007). The latter model suggests SSW to NNE inflow along a common feeder zone from an evolving mafic source 20 km to the south, forming two gently-dipping sheets (Stevenson and Bennett 2011). Both Richey (1928) and Stevenson and Bennett (2011) depict the outcropping granite facies along topographic cross-sections that they interpret as an erosion level representing the roof zone of a pluton. Mattsson *et al.* (2020) mapped fracture patterns in the contact-metamorphic aureole to constrain deformation caused by magma emplacement, and found a lack of pluton-wide rotational deformation in the roof zone. They inferred that emplacement of the Mourne Mountains granites involved asymmetric 'trap-door' floor subsidence with wall deflection along a fault in the NE and local roof uplift in the SW.

Analytical methods

As part of the Tellus survey, stream–sediment samples comprising the <150- μm fraction were gathered by wet sieving on site from first- and second-order streams at an average density of 1 sample per 2.15 km². Soil samples were collected at 35–50 cm depth (referred to by BGS as the 'S' sample) and the <2-mm fraction was analysed. The survey methodologies followed the established sampling and analytical protocols of the GB Geochemical Baseline Survey of the Environment (G-Base) (Johnson *et al.* 2005; Smyth 2007; Young *et al.* 2016). The stream–sediment was analysed by XRF and fire assay while 'S' type soil samples were analysed by total acid digestion and fire assay. The elements under investigation were Ag, Al, As, Au, Ba, Bi, Br, Ca, Cd, Ce, Co, Cr, Cs, Cu, Fe, Ga, Ge, Hf, I,

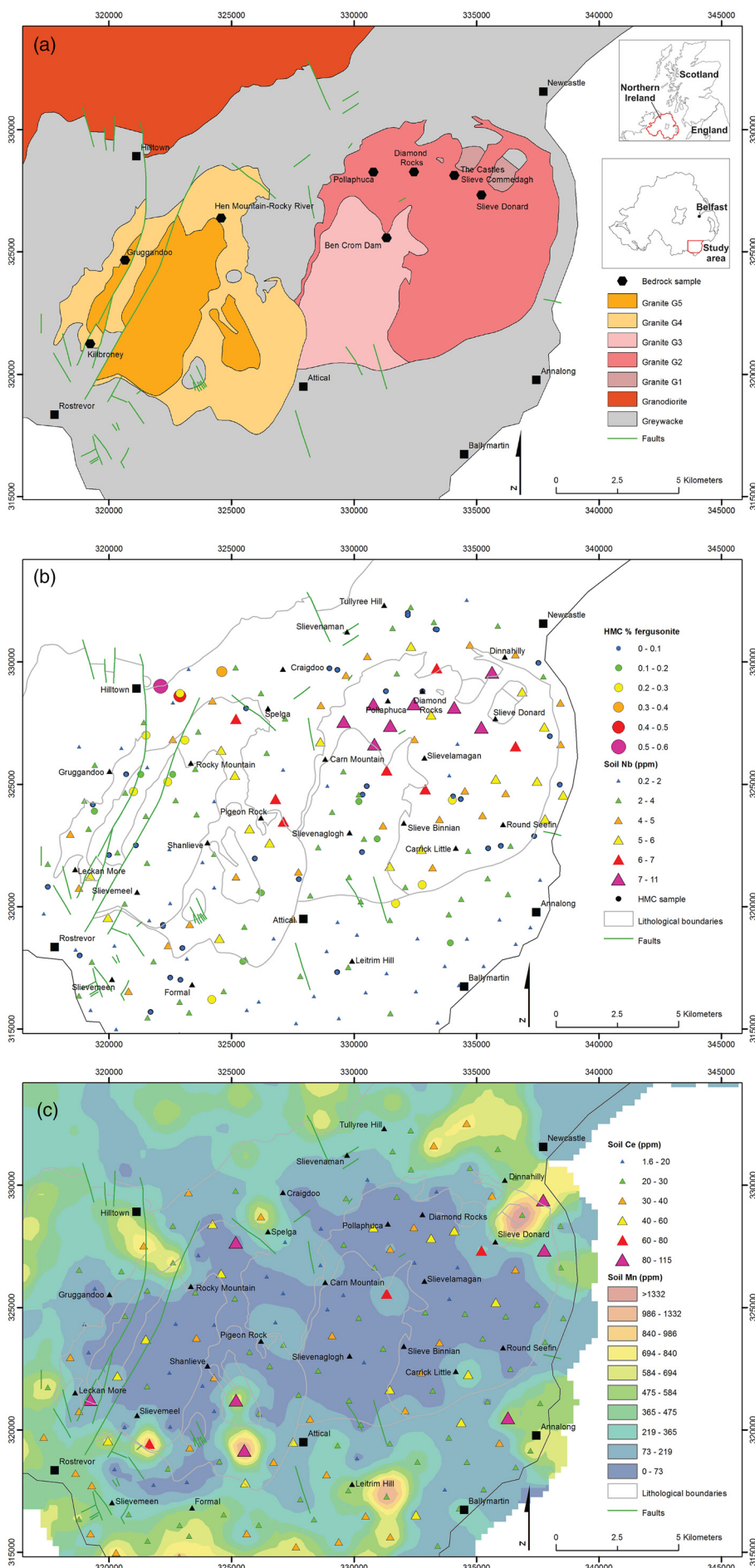


Fig. 1. (a) Geological map of the Mourne Mountains granite complex showing the locations of the geochemical anomalies in the Tellus deep soil data that were investigated in the field, as summarized in Table 1. Inset maps showing location of Northern Ireland and the study area. Geological linework based upon Hood (1981). © Crown copyright and database right (2013), (b) Map of Nb point anomalies (ppm) in Tellus deep soil Multi-Acid (near Total) ICP data (triangles) and the occurrence of fergusonite in heavy mineral concentrates (circles, courtesy N.Moles unpublished data), (c) Map of gridded Mn concentration (ppm) in Tellus deep soil Multi-Acid (near Total) ICP data overlain by point Ce deep soil data (ppm) – small isolated occurrences of Ce and Mn (deep soil) enrichments in both the western and eastern Mournes.

Table 1. Tellus soil geochemical anomalies that were examined during field investigations

Anomaly location, grid reference	Deep soil anomalies	Description of locality
WM1 Gruggandoo 320660 324653	Sr, V	Shear zone with clay formation, G4 granite north of Tellus data point
WM2 Hen Mountain-Rocky R 324585 326389	Ce, Mn	Poor bedrock exposure; leucocratic granular fine-grained drusy G4 granite
WM3 Kilbroney 319239 321240	La, Ce, Y, Yb, U, Th	Veins hosted by granites in fault zone close to contact between G4 (granite, drusy granite, pegmatite) and hornfels
EM1 Diamond Rocks 332451 328274	Nb	Drusy G2 granite: locally biotite-rich granite and pegmatite, beryl noted
Ben Crom Dam 331334 325571	Ce	Large moraine – anomaly cannot be traced: no samples
EM2 Pollaphuca 330796 328267	La, Y, Yb, P, As, Sn	Replacement zones with peripheral greisens and veinlet
EM3 Slieve Donard 335208 327324	La, Ce, Y, Yb, U, Be, Mn	No bedrock exposures: numerous granite boulders likely to relate to anomaly, likely to be local bedrock
EM4 The Castles 334099 328133	Th, Nb, Li	G2 biotite-rich granites, drusy granites and pegmatites; beryl noted
EM5 Slieve Commedagh 334099 328133	As above	G1 granites and granitoids outcropping upslope from The Castles

WM denotes a Western Mourmes location and EM denotes an Eastern Mourmes location. The term 'deep soil' refers to the 35–50 cm soil depth referred to by BGS as the 'S' sample.

K, La, Mg, Mn, Mo, Na, Nb, Nd, Ni, P, Pb, Pd, Pt, Rb, Sb, Sc, Se, Si, Sm, Sn, Sr, Ta, Te, Th, Ti, U, V, W, Y, Zn and Zr (Johnson *et al.* 2005). The stream-sediment and soil geochemical data sets from the Tellus Survey were imported into ArcMap GIS software as both raw data points and gridded maps. The maps used to identify geochemical anomalies were generated using Esri ArcMap GIS version 10.2, focusing on the traditional GIS workflow in a 2D environment. A subset of the Tellus point data for the study area was created to aid identification of anomalies across the Mourmes. The point anomaly data for each analyte was classified into six class ranges, with larger intervals for low and high data tails and shorter intervals to split the modal results, as depicted on Figure 1b and c, represented by proportional and/or colour-coded symbols.

Polished thin sections of rock samples (from locations depicted in Fig. 1a) were investigated in the first instance with either a JEOL JSM-5400LV Low Vacuum SEM-EDS system at the Camborne School of Mines, University of Exeter and/or a LEO 535VP variable pressure SEM-EDS system at the British Geological Survey petrography and microanalysis laboratories. Subsequently QEMSCAN®, the Quantitative Evaluation of Minerals (QEM), was used to produce complete mineral maps of whole polished rock thin sections of a total of 5 representative bedrock samples. The QEMSCAN® 4300 at the Camborne School of Mines, University of Exeter, analysed samples with an X-ray pixel spacing (resolution) of 10 µm. For critical metal-bearing minerals with grain-size near to or beneath the resolution of the QEMSCAN®, high-precision element maps of fine-scale structures were obtained using the LEO 535VP variable pressure SEM. The QEMSCAN® analytical technique, including details of the instrument and methods used, are outlined in published literature (Andersen *et al.* 2009; Haberlah *et al.* 2011; Rollinson *et al.* 2011; Santoro *et al.* 2014). Specifically, this technique correctly identify the minerals or phases by comparing collected X-ray spectra from each analysis point (pixel) to a mineral database (SIP) that is customised using the results of mineral analysis (EDXA and EPMA, as described below). Depending on the size of the section, between 6 million and 6.5 million X-ray analysis points were obtained during an 11–12 hour field image scan to generate a statistical analysis of grain-size and mineral abundance. This study required development of the database to accurately identify the unusual minerals present in the samples, such as the REE and As minerals. One further advantage for this study was the ability to obtain mineral association data,

which is based on the adjacency of the analysed pixels, measured in the horizontal plane and displayed as a percentage.

Mineral chemistry was analysed for 8 rock samples (from locations in Fig. 1a) in the first instance using a FEI Quanta 600 environmental scanning electron microscope (ESEM) fitted with an Oxford Instruments X-MAX large area (50 mm²) silicon drift detector (SDD) energy-dispersive X-ray microanalysis (EDXA) system, run with Oxford Instruments' INCA (v.4) software at the British Geological Survey. Operating conditions were a high vacuum (1.2×10^{-4} Torr), accelerating voltage of 20 kV, at the instruments' optimal analytical working distance of 10 mm with a detector take-off angle of 45°. Analytical live-times of 30–60 s were used for spot and small area (5 µm across) raster analyses. Details of beam current control, EDXA detector noise reduction and standards are summarized by Walters *et al.* (2013). INCA software applies 'phi-rho-z' matrix correction methods (after Pouchou *et al.* 1990) and uses multiple least squares for peak deconvolution. Procedures used for the SEM-EDXA quantitative microanalysis were in line with those recommended by the ASTM Standard (ASTM-Standard-E1508 2012). Prior to analysis, beam stability was established by initial monitoring of specimen current over an extended period (30 min) whilst in spot mode on a Co primary standard. As final confirmation of stability, three consecutive analyses run on the Co primary standard were required to return totals within a 1% range before proceeding and repeat Co standard calibrations were performed every 20 min to monitor and correct for beam drift. The methodology produces comparable quality results to conventional WDXA major element analysis and for total REE + Y, but resolution of REE and other metals analysis required electron probe microanalysis (EPMA) with manual corrections for overlaps in REE wavelength peaks using the JEOL JXA-8200 Superprobe at the Camborne School of Mines, University of Exeter. Operating conditions were an accelerating voltage of 20 kV, 10 nA current and a 5 µm spot size and a combination of natural and synthetic mineral standards were used. Detection limits (2σ) were between 0.19 and 0.44 wt% for REO, <0.18 wt% for oxides of Y and Yb, and <0.07 wt% for oxides of Th and U. The location of wavelength dispersive analytical points (EPMA) were selected as far as possible to be the same as used for the SEM analysis, to facilitate inter-laboratory and methodological precision. Correlation between the methods resolved and confirmed the concentrations of La, Ce, Pr, Nd and Sm with confidence, while Y, Gd and Dy often occurred in concentrations above but close to the

detection limits of the JEOL JXA-8200 Superprobe. The minerals hosting critical and associated metals, particularly those occurring as inclusions and secondary minerals were frequently too fine-grained for reliable LA-ICP-MS analysis.

Regional survey results and sampling programme

The chemistry of deep (S, deeper collection point) soil and stream sediment samples collected and analysed during the Tellus project

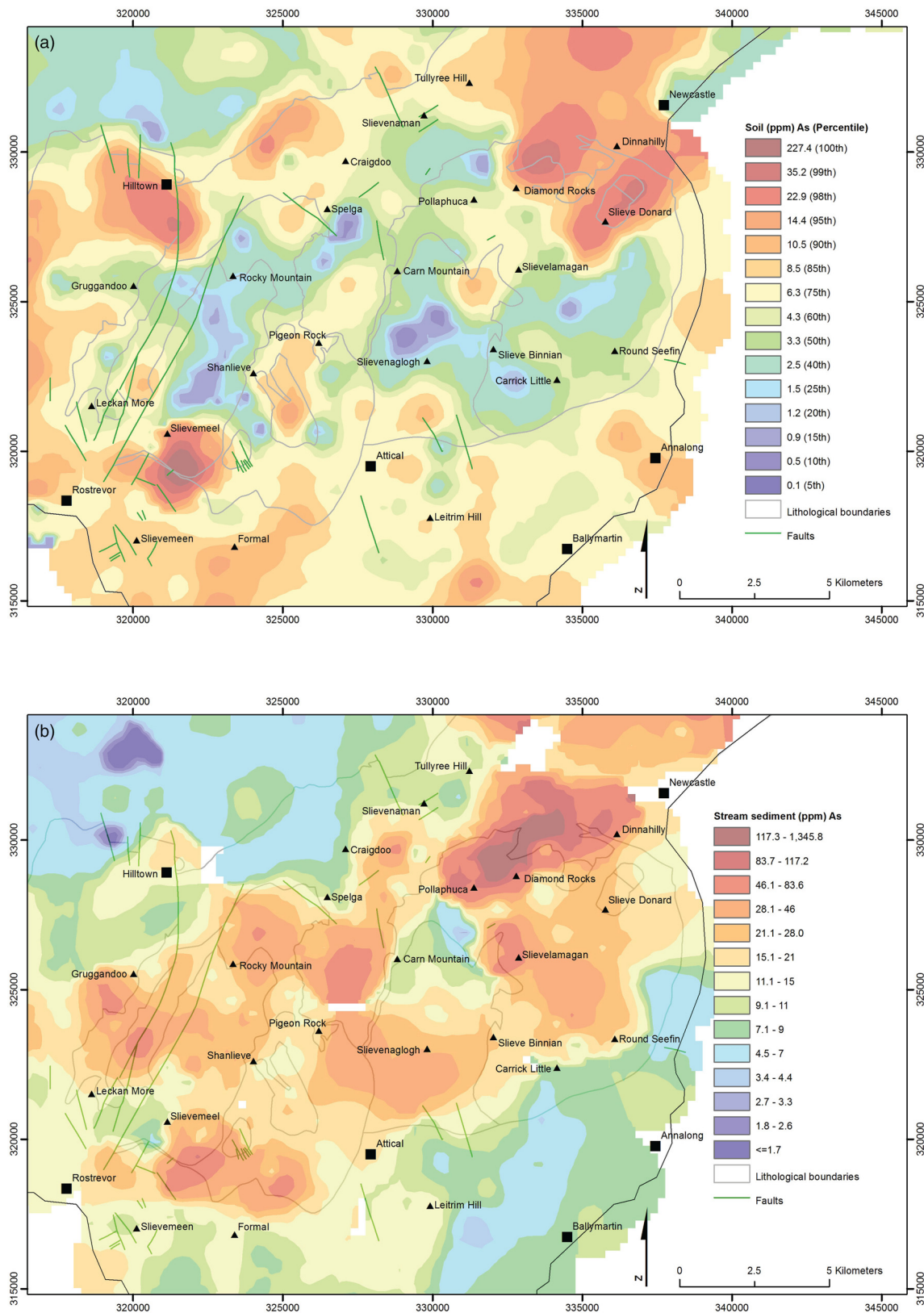


Fig. 2. Arsenic (As) anomalies in soil and stream data. (a) Map of gridded As concentration (ppm and as percentiles) in Tellus deep soil Multi-Acid (near Total) ICP data – three significant As (deep soil) enrichments are located in both the western (Slievemeel) and eastern Mournes (NE of diamond rocks and Slieve Donard), (b) Gridded map showing a spatially large positive As (stream sediment) anomaly in a SW-NE lineament across the western and eastern Mournes, but particularly pronounced in the northern part of the eastern Mournes. Geological linework based upon Hood (1981). © Crown copyright and database right (2013).

show that the eastern Mourne granites are generally more enriched in critical and industrial metals (for example, REE, Nb, As, U) than the western Mourne granites (Figs 1b, c and 2a, b). Prominent patterns of soil (and stream sediment) chemistry were identified by inspection: concentrations of metals were usually 4 to 6 times (e.g. up to 11 ppm Nb, 115 ppm Ce, and 227 ppm As) higher in soil or more than 15 times higher in stream sediment (up to 1346 ppm As) than background concentrations (up to 4 ppm Nb, 30 ppm Ce, 14 ppm As – 84 ppm As in streams, Fig. 1b, c; Fig. 2a, b). (1) A large curvi-linear array of positive chemical anomalies that strikes west–east across the eastern Mourne (Fig. 1b), in or near the roof zones of the earliest intrusions (Fig. 1a) is characterized by significant Nb enrichment, coupled to Th concentration (\pm Ce and other elements), but it is not strongly correlated with the occurrence of fergusonite in heavy mineral concentrates nor with soil depth. (2) Isolated anomalies (e.g. REE and U, Th, V and Cr) associated with NNE–SSW-trending structures in the western Mourne had less Nb than in the eastern Mourne. V and Cr are not considered further in this survey as they are considered to relate to glacial transport of material (as erratics) from granodiorite to the north (McCabe 2008), or more locally the dykes that intrude the granite. (3) A group of sporadic anomalies (Ce–Mn) in the southern part of the western Mourne were neither extensive nor associated with known structures (Fig. 1c) and had less prominent Th and Nb signatures than elsewhere. In addition, soil and stream sediments had chemical compositions that defined different source patterns for As. High concentrations of As were distributed in deep soil at Slieveveel in the SW (up to 227 ppm), and in NE–SW-trending lineaments (up to 35 ppm) to the NE of Diamond Rocks and Slieve Donard (Fig. 2a). The soil As enrichment is not directly comparable with stream As enrichment, having a linear pattern that strikes WSW–ENE and cuts diagonally across the generally north-flowing drainage in the NW of the eastern Mourne (Fig. 2b). The result demonstrates that chemical anomalies in bedrock (Fig. 2a) are successfully identified using soil analysis even where there is no surface expression, and that anomalies in stream sediments (Fig. 2b) can effectively identify where mineralization in rock exposures interacts with waters flowing through stream cuttings and where anthropogenic (quarrying) activity has redistributed metals.

A total of 8 soil geochemical anomalies (Fig. 1a, Table 1) were selected as case studies on the basis of high concentrations of critical elements relative to the majority of soils overlying granite. Positive anomalies in REE (Ce, La) concentrations correlated well with other analytes such as Th and Nb supporting the prospectivity of the areas initially identified, although some notable variations in the anomalies were apparent (Table 1). Samples that were representative of in-situ bedrock variation were collected in the vicinity of 5 anomalies. Sampled granitic rocks were not in-situ at two of the anomalies (Hen Mountain in the western Mourne and Slieve Donard in the eastern Mourne) where float boulders in the drift material were sufficiently prominent to influence the chemical anomalies in deep soil. It is likely that the samples taken at these two sites represented bedrock lithologies, since glacial transport was to the south during the last (late Midlandian) glaciation (Bazley 2004) and the samples matched the surrounding bedrock but not the bedrock in the path of glaciers to the north. No samples were taken at one of the anomalies (Ben Crom Dam, Fig. 1a), which was identified as a lateral moraine (Wilson 2004) such that it would not be possible to identify a specific bedrock source. The association of anomalies with the roof zones of early intrusions and with structural lineaments was used to develop a sampling programme that targeted pegmatites/drusy granites zones, greisen veining that overprinted granites, and fault zones that showed evidence that they had acted as fluid pathways (Table 1).

The lithological samples from the eastern Mourne are dominated by G2 granites (Hood 1981), of which prominent outcrops with associated talus slopes occur in close proximity to soil geochemical

anomalies at Diamond Rocks and The Castles of Commedagh (Fig. 3a). The granites contain drusy patches and sometimes grade into pegmatite. Discrete pegmatite veins were not observed during the field sampling campaign. Anomalies for Nb, Y and La in the multi-element stream sediment Tellus data, and anomalies for Ce, La, Y, Yb and Li in the deep soil geochemical data were observed at localities that have been noted for a century for the occurrence of tourmaline, topaz, beryl and zinnwaldite (Richey 1928). G1 granites that outcrop on mountain summits above Diamond Rocks and the Castles were also sampled to investigate the significant heterogeneity in the soil chemistry. The G4 granites in the western Mourne that were sampled were finer-grained overall than the G1 and G2 granites, but they also locally graded into drusy granites and pegmatites, and correlated with highly variable deep soil anomalies. Grain-size variations have been documented throughout the G1 to G5 intrusions and have been related to internal contacts (Hood 1981; Gibson 1984; Meighan *et al.* 1984). Three different types of hydrothermal veins were sampled in both the G2 and G4 granites at the localities investigated. Prominent iron-rich veins of variable thickness were flanked by a wide zone of microveining at Pollaphuca in the G2 granite (Fig. 3b). Small epidote veins were associated with anastomosing bands of clay (Fig. 3c) weathered from the detritus of cataclasis in an extensive shear zone at Gruggandoo. Microveins and greisen veins (Fig. 3d) were located on the edges of a topographical depression associated with a major fault zone at Kilbroney.

Rock textures and mineral assemblages

Granites, drusy granites and pegmatites

Table 2 and Figure 4 show the relative volumes of the minerals identified using QEMSCAN® analysis. Three samples are 2-feldspar subsolvus biotite granites that generally have silicate accessory phases dominated by amphibole in the least fractionated, oldest granites (e.g. G1, Figs 3a, 4a) and by muscovite in the more fractionated younger granites (e.g. G4). G1 granite samples (EM5, Figs 4a, 5a) are highly variable allanite-bearing, amphibole-biotite granites and syenogranites. The G2 granites (EM1, EM3, EM4, Table 1) are dominantly biotite-granites with drusy cavities dominated by smoky quartz, feldspar and occasional beryl and topaz. Patches of pegmatite in gradational contact with G2 and G4 granite had variable grain-sizes, with feldspar crystals observed up to 5 cm in length. Microscopic rock textures are dominated by spectacular intergrowths of all the major rock-forming minerals (Fig. 5b) and some of the accessory minerals. Graphic, radiate graphic and micrographic textures are the most common but myrmekitic textures are frequently observed between plagioclase and quartz, between biotite and quartz or between biotite and alkali feldspar. Very rarely, micrographic intergrowths of cuneiform appearance occur between zircon with various small (<10 μ m) inclusions and either quartz or biotite. Zircon, magnetite and allanite are present in all the granites sampled but there is great variation in the rest of the accessory mineral assemblage that has a grain-size <10 μ m, which is smaller than the resolution of the QEMSCAN® analysis used in this study. G1 granite sample EM5 (Fig. 5a) contains allanite at 0.12 vol% (Table 2), the greatest volume of rare-earth minerals >10 μ m. In contrast, G2 granite samples contain a range of rare-earth minerals that constitute a much smaller proportion of the total rock.

The observation that high atomic mass minerals were preferentially hosted in mafic silicate host minerals (Figs 4a, b and 5a) was tested using the mineral association data from the QEMSCAN® analysis. Figure 4a shows that the G1 granite sample (EM5-2) has euhedral allanite in apparent association with biotite, which is 3.57 vol% of the mineral assemblage, and chloritised calcic-amphiboles (false colour green 0.8 vol% and red 0.97 vol%), which comprise 1.77 vol% of the mineral assemblage (Table 2).

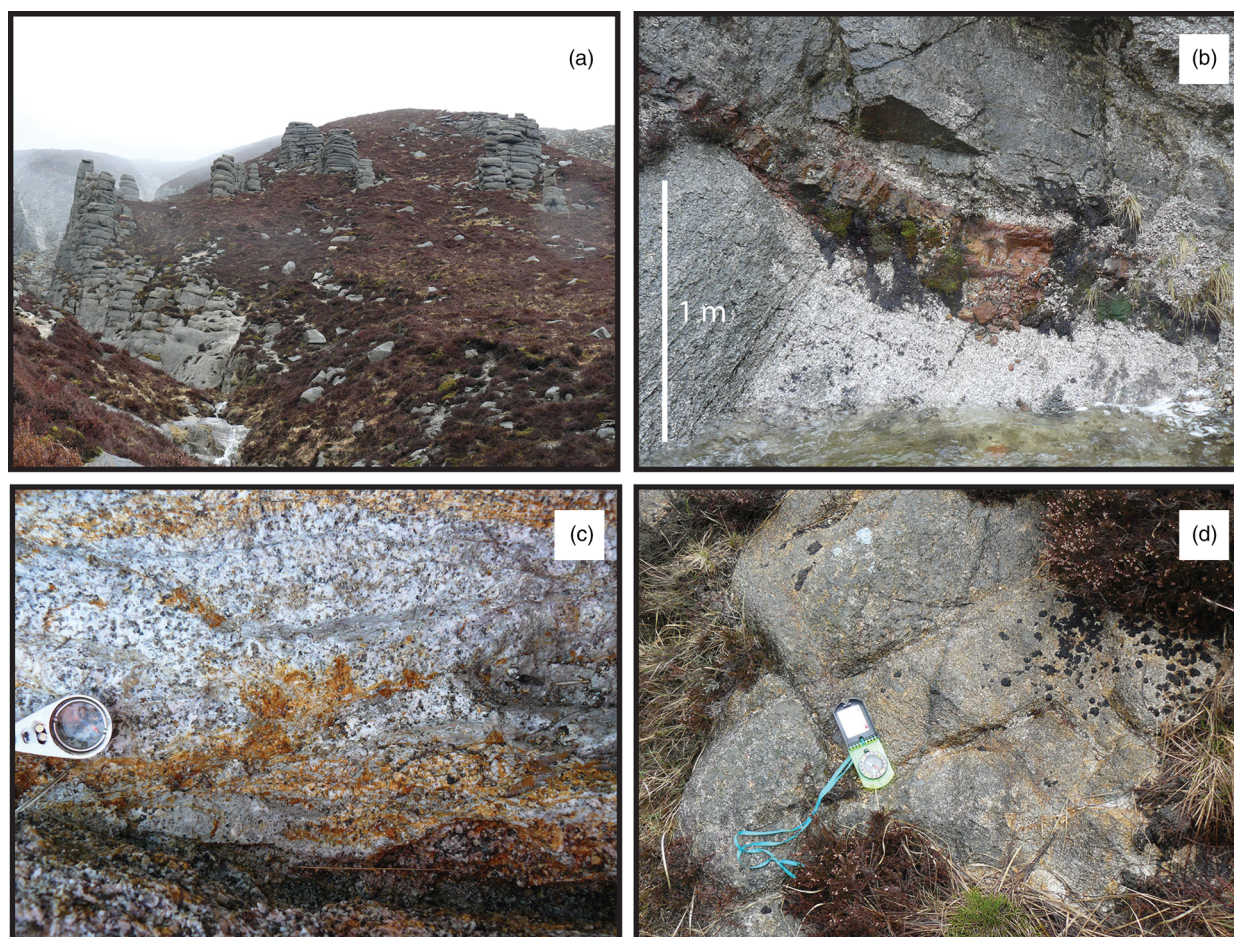


Fig. 3. Field photographs of sample localities and lithologies: (a) G2 granite outcrop at the Castles of Commedagh (EM4), (b) Zone of replacement with peripheral veining in G2 granite at Pollnaphuca (EM2), (c) Shear zone with local clay formation after gouge in G4 granite at Gruggandoo (WM1), (d) Greisen veins near a fault zone at Kilbroney (WM3).

Overall, 65.3% of allanite, 44.0% zircon, 48.4% apatite and 50.2% magnetite are in association (adjacency) with the total mafic silicate mineral assemblage, i.e. amphibole (0.97 vol%) + biotite (3.57 vol%) + chlorite (0.8 vol%), which is 5.34 vol% of the sample. Likewise, G2 granite (sample EM4A, Fig. 4b) comprises minor accessory minerals aphanite, thorite, zircon and magnetite with association of >40%, monazite with association of >55%, and ilmenite and allanite with association of >65% with the mafic silicate minerals that together (1.99 vol% biotite and 1.58 vol% chlorite, Table 2) constitute 3.57% of the sample. Despite the lower abundance of the mafic silicate minerals, tourmaline is more abundant (0.22 vol%, Table 2) and has 75.2% association, dominantly with chlorite. G4 granite (sample WM2) contains a lower abundance of mafic silicate minerals (total biotite and chlorite = 2.16 vol%, Table 2) than G1 and G2 granites (samples EM5-2 and EM4A) and, consequently, the association between the accessory mineral assemblage and mafic silicate minerals is not particularly strong. However, titanite and allanite occur in volumes of 0.03 and 0.01%, and have adjacency of 43.7 and 41.7%, respectively.

Drusy infill and granite replacement

Mn-rich phases that were identified by QEMSCAN® analysis in G4 granite (asterisk, Fig. 4c; Fig. 6a) have a distribution that is clearly delineated by quartz, K-feldspar and plagioclase: they are interpreted as infill of a drusy cavity, such as that visible in the G2 granite (Fig. 4b). False colour element maps (Fig. 6b–d) show that biotite/chlorite crystals occur in the cavity, which is dominated by a porous and largely amorphous network of manganese-rich to

cerium-rich mineralization. Semi-quantitative chemical analyses show that the composition is consistently dominated by manganese hydroxide with up to 5 wt% PbO₂, 2–4 wt% Al₂O₃, 1–2 wt% BaO, an average of 1 wt% CaO and an average of 0.5 wt% of each of K₂O and MgO. Traces of arsenic, sulfur, bromine and chlorine are common throughout the mineralization. Ce concentration is highly variable from 0 to >20 wt% Ce₂O₃. The host rock does not appear to have undergone any large-scale replacement or metasomatism other than the infill mineralization, which correlates with a Ce-only soil anomaly (WM2, Table 1) in the Tellus deep soil data. There are no apparent minerals that can account for the Ce and Mn anomaly at the locality, other than the druse-infill mineralization. The strength of the association between the Ce and Mn anomalies was tested using the Tellus data (Fig. 1c). The local manganese enrichment is not visually pronounced at Hen Mountain but there are three other notable coincident Ce-Mn anomalies in the Tellus data (to the west of Attical and to the south of Shanlieve and Slievemeel; Fig. 1c) that may be caused by a similar style of mineralization. It is possible that the four anomalies represent a localized phenomenon related to late-stage magmatic-fluid processes.

Figure 4d and e show QEMSCAN® mineral maps of samples from the greisen border and the iron-stained centre of the replacement vein at Pollnaphuca (locality EM2, Fig. 2b), which correlates with a spatially extensive arsenic anomaly that is most prominent in stream sediment data (Fig. 2b). Comparison between the EM2 samples and the G2 granite host rock (similar to that depicted in Fig. 4c) illustrates that the earlier stages in the progressive metasomatism of the G2 granite are accompanied by the development of extensive micro-veining (sample EM2a_3, Figs 4d, 5c) and that the later stages of

Table 2. Modal mineralogy (crystals >10 µm grain size) for samples analysed using the QEMSCAN®, calculated by pixel counting to generate percentage mineral volume

Mineral volume %	EM5-2	EM4a	WM2	EM2a_3	EM2a_1
Allanite (Ce,Ca,Y) ₂ (Al, Fe) ₃ (SiO ₄) ₃ (OH)	0.12	0.01	0.01	0.02	
Almandine/chlorite * ¹	0.80	1.58	1.39	3.06	2.73
Apatite Ca ₅ (PO ₄) ₃ F	0.08				
Arsenopyrite FeAsS					0.57
Arseniosiderite Ca ₂ Fe ₃ (AsO ₄) ₃ O ₂ ·3H ₂ O					0.87
Ashanite (Nb,Ta,U,Fe,Mn) ₄ O ₈		<0.01			
As Al phase					0.03
Biotite	3.57	1.99	0.77	4.58	1.19
Ca Fe Al silicates	0.97				0.05
Cassiterite SnO ₂		0.01		0.02	
Chenevixite Cu ₂ Fe ₂ (AsO ₄) ₂ (OH) ₄					<0.01
Chernovite-(Y) (Ce,Y)AsO ₄					0.01
Cu (Fe) Sulfides					<0.01
Fe-Ox(Mn)/CO₃	0.01	0.02	0.11	0.05	0.05
Fergusonite Y(Nb,Ta)O ₄		<0.01			
Ilmenite FeTiO ₃	0.09	0.03	0.09	0.04	0.02
K-feldspar	44.57	38.42	43.75	32.16	0.53
Kaolinite	0.04	0.20	0.03	1.15	0.74
Monazite (Ce,La,Nd,Th)PO ₄		0.01	0.01	0.03	0.01
Mn-phases			0.11		
Muscovite			0.12	2.99	2.86
Pharmacosiderite KFe ₄ (AsO ₄) ₃ (OH) ₄ ·6–7H ₂ O					0.95
Plagioclase feldspar * ²	16.54	16.55	18.00	7.18	0.87
Quartz	33.06	40.89	35.52	47.72	74.29
Rutile TiO ₂		0.02		0.05	0.04
Scorodite FeAsO ₄ ·2H ₂ O					4.59
Tennantite (Cu,Fe) ₁₂ As ₄ S ₁₃					0.02
Thorite (Th,U)SiO ₄		<0.01		<0.01	
Ti-magnetite Fe(Fe,Ti) ₂ O ₄			0.03		
Titanite CaTiSiO ₅	0.01		0.03		
Topaz Al ₂ SiO ₄ (F,OH) ₂				0.56	8.63
Tourmaline		0.22		0.30	0.77
Xenotime (Y,REE)PO ₄				<0.01	
Zircon ZrSiO ₄	0.04	0.01	0.02	0.03	0.01
Others	0.08	0.02	0.02	0.04	0.18

Samples EM5-2, EM4a and WM2 are G1, G2 and G4 granites respectively. Samples EM2a_3 and EM2a_1 are from the margin and the core of replacement vein mineralization that is hosted by the G2 granite (EM2 Pollaphuca, Table 1).

*Note that: 1, the QEMSCAN® cannot differentiate between almandine garnet and chlorite, the latter being the more common phase in these rocks. 2. Plagioclase feldspar is pure albite in EM2 samples.

metasomatism involve total replacement of the rock (sample EM2a_1, Fig. 4e). Plagioclase and quartz contents have an inverse relationship (Table 2) and a particularly large increase in the abundance of quartz or an alternative silica polymorph from 47.72 vol% in the greisen (sample EM2a_3, Table 2) to 74.29 vol % in the centre of the replacement zone (sample EM2a_1, Table 2) occurs at the total expense of both feldspars (Fig. 4e). Subsequently, with increased open system metasomatism, topaz starts to grow (sample EM2a_1, Fig. 5d) with increasing grain-size and abundance that varies from 0.56 vol% at the margin of the replacement zone to 8.63 vol% in the centre (Fig. 4e, Table 2). Coupled with the alteration of biotite ± amphibole to chlorite, the mineralogical changes clearly demonstrate that the rock has been silicified with remobilization/leaching of K and Ca, by F-rich hydrous fluids. The mafic minerals start to be replaced by high atomic mass minerals close to the margin of the veins in the greisen (Fig. 5c) and cassiterite is preferentially located in mineral pseudomorphs and microveins in greisens – cassiterite was not recorded in the core of the replacement mineralization. The high atomic mass minerals in the core of the replacement zone are dominated by the As-rich minerals scorodite, chernovite (Ce,Y)AsO₄, arseniosiderite, pharmacosiderite. In addition, a variety of unresolved mineral phases, some containing As and Al, were identified (Table 2).

Hydrothermal veins associated with tectonic lineaments

Samples from the locations of chemical anomalies in Tellus deep soil data along NNE-SSW-trending tectonic structures in the western Mourne (Table 1, Figs 1, 2) included G4 biotite granites with kaolinised feldspars and gouge that has altered to a soft plastic clay in anastomosing shear zones, which are cut by quartz-epidote veins on slickensided fault planes (Fig. 3c, d). High atomic mass minerals are dominantly associated with biotite (Fig. 7a), as in G2 granites. Chlorite occurs in radiating aggregates replacing biotite, infilling cavities and along grain boundaries (Fig. 7b) and clusters of prismatic epidote crystals grow inwards from the margins of veins and from quartz crystal surfaces (Fig. 7c, d). Veined granites at localities WM1 and WM3 (Table 2, Figs 1, 2) contain sub-10 µm grain-size REE-minerals, dominantly monazite. The grain-size of minerals hosting the critical metals is smaller than the resolution of QEMSCAN® analysis used in this study.

Mineral textures and chemistry

Mineral chemistry (Tables 3–6) was analysed for 8 of the 25 samples that were investigated petrographically: 3 samples of granites (G1, sample EM5-2; G2, sample EM4a; G4, sample

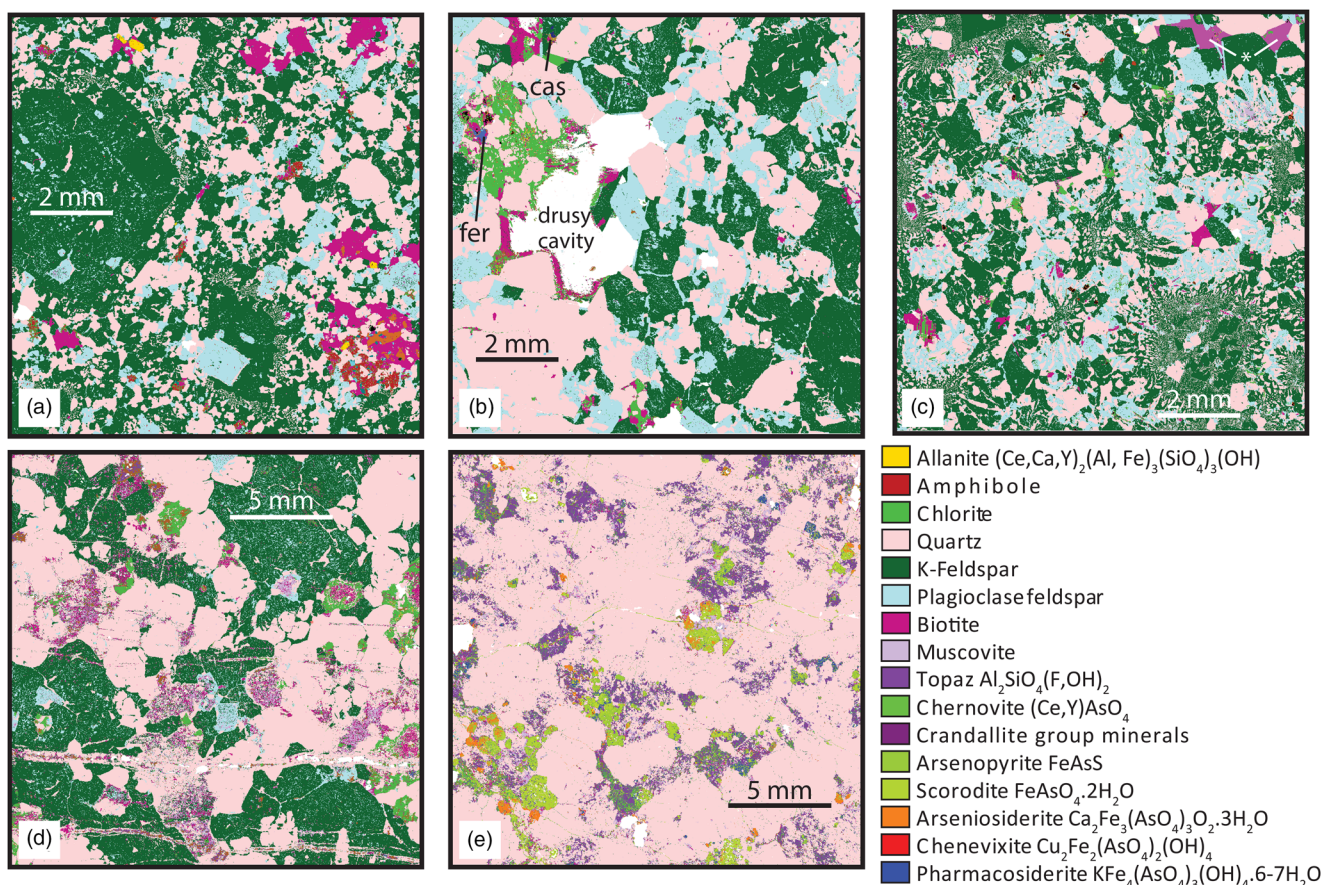


Fig. 4. QEMSCAN® mineral maps of rock textures in Mourne granites: (a) G1 granite (sample 5_2) has orthoclase megacrysts with radiating graphic texture and allanite-(Ce) in close association with biotite and chloritised amphiboles, (b) G2 granite (sample EM4A) showing hypidiomorphic granular texture with accessory anhedral fergusonite-(Y) (fer) and cassiterite (cas), (c) G4 drusy granite with sparse biotite and muscovite (sample WM2), which has extensive micrographic texture radiating from euhedral k-feldspar crystals and drusy cavities infilled with Mn-rich phases at the top of the section, marked with an asterisk, (d) G2 granite (sample EM2a_3) greisen containing cassiterite-bearing quartz microveins, (e) G2 granite (sample EM2a_1) in the core of the replacement mineralization, which is dominated by arsenic-rich minerals. Images (d) and (e) illustrate progressive metasomatism of granite, resulting in replacement of feldspars and mafic silicate minerals by quartz and an As-rich mineral assemblage, respectively.

WM2); 3 samples across the replacement vein structure cutting the G2 granite (samples EM2a_1-3); 2 samples from veins through the G4 granite (samples WM1e and WM3d) in the western Mourne.

Host silicate minerals

Other than myrmekitic textures, quartz, and partially-altered plagioclase and potassium feldspars have consistent features across most samples. The exception is where G2 granite has been extensively metasomatised at Pollaphuca: feldspar is progressively altered to pure end member albite (ESEM analysis) typical of metasomatic processes, and chemical impurities in quartz (or other silica polymorph) increase towards the centre of the mineralization. Semi-quantitative analysis shows that the silica polymorph in the most arsenic-rich part of the mineralization where cassiterite is not a stable mineral phase (sample EM2a_1, Fig. 4e) contains 1.3–1.5 wt % In_2O_3 (typically occurring at concentrations of about 0.05 ppm In in continental crust) and 0.7–1.1 wt% SnO_2 . Topaz that has crystallized in metasomatised granites (Fig. 5d) contains variable quantities of trace iron (<0.8 wt% FeO total) in the core of the mineralization, but topaz is Fe-absent on the margins.

Amphiboles in sample EM5-2 (Figs 4a, 5a) are potassium- and chlorine-rich hastingsite (Table 3), a sodium-bearing calcic amphibole that contains approximately 1 wt% MnO. Primary biotite in the G1 and G2 granites is close to annite in composition (e.g. Mg # = 0.14 for G1 biotite; 0.04 for G2 biotite), contains

chlorine and has average MnO concentration from 0.5 wt% (G1) to 0.35 wt% (G2). In contrast, metasomatised biotite is end-member annite to arsenic-bearing annite and contains no manganese or chlorine (Table 3). Chlorite shows a converse relationship to biotite. It contains no Cl or Mn in unmetasomatised G2 granite samples (EM4a) but greisens contain chlorite that is relatively enriched in Mn (typically 0.45 wt% MnO) and Cu (2–3 wt% CuO) (EM2a_2, Table 3).

Biotite on the margins of a quartz-cassiterite vein has undergone dissolution, with some crystals acting as the location for precipitation of secondary high atomic mass minerals, including Ti-magnetite, zircon, cassiterite and monazite-(Ce) (Fig. 8a). Transects across zoning in the rim of biotite (Fig. 8b) show a negative correlation of FeO (total) with alumina and silica, constant K_2O concentration and an iron-rich convoluted overgrowth, most apparent in transect 2 (Fig. 8c). Thus this zonation is not due to the formation of chlorite, which is common elsewhere in the sample, but the replacement of biotite by mica close to a muscovite composition by metasomatic processes. The abundance of muscovite reaches 3% in metasomatised G2 granite (Table 2) in marked contrast to the magmatic occurrence of muscovite that is restricted to G4 granites.

At least three generations of secondary epidote ± allanite are apparent in veined samples. (1) Large epidote crystals occur in clusters of fibrous or euhedral prismatic and sometimes zoned crystals radiating from the margins of, and crystal faces within, macroscopic quartz-epidote veins (Fig. 7c, d). (2) Small subhedral-

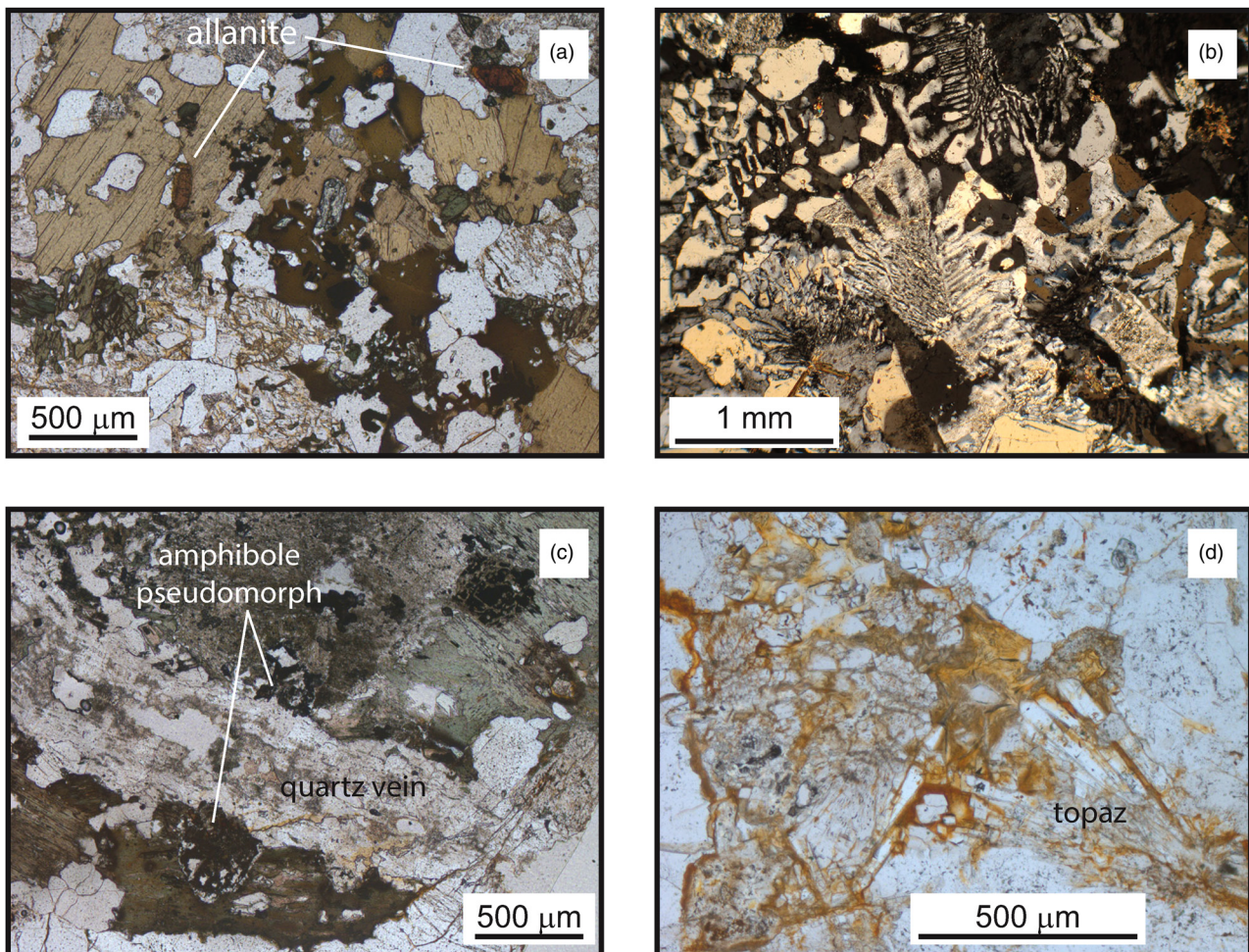


Fig. 5. Microphotographs of granitoid lithologies: (a) Phaneritic texture in G1 allanite-(Ce) -biotite-(amphibole) granite, EM5-2, (b) Radiating graphic and myrmekitic texture, EM1b, (c) An amphibole crystal is split by a quartz vein and replaced with an assemblage dominated by cassiterite and monazite-(Ce), sample EM2a_3, (d) Large radiating aggregates of topaz in association with Fe-enrichment, sample EM2a_1.

anhedral (replacement) epidote and small euhedral Ti- and Mn-zoned epidote crystals (Fig. 9c) occur in chlorite-dominated pockets along grain boundaries, such as that shown in Figure 7b. (3) Tiny radiating acicular aggregates of allanite occur in association with the small zoned epidote crystals (Fig. 7c, d). Other than the zoning in small euhedral crystals, the composition of the types of epidote is largely consistent (Table 3).

REE-silicate minerals

Large primary allanite-(Ce) crystals in the G1 granite have relatively large grain-size (up to 200 μm long) and prominent chemical zoning (Fig. 9a, b): the REEs, particularly La, decrease from the core to the rim, while Th concentration increases (Fig. 9e). The internal zonation is repeated in some crystals (Fig. 9b, Table 4) where a positive Ce anomaly occurs (Fig. 9f) for negative anomalies of other REE, suggesting oxidation of Ce to 4+. The Ce anomaly corresponds with an increase in Si, Al, Ca and Fe concentrations, and decrease in Ti concentration (Fig. 9f). The data are consistent with episodic magmatic recharge by an oxidized silicate magma. A small overgrowth (analysis point 13, Fig. 9f) has elevated REE and Th compared to the crystal rims (analysis point 12, Fig. 9f) due to small scale recrystallization processes as a consequence of either magmatic-fluid migration or post-consolidation fluid migration. Secondary allanite-(Ce) has been observed in infrequent localized pockets of fine-grained porous material replacing biotite in both the G2 granite at Diamond Rocks and in the G4 granite at Hen Mountain. Relative to the primary allanite-(Ce) in G1 granite, the

secondary allanite-(Ce) in the G4 granite has lower TiO_2 and MgO , and higher Al_2O_3 and CaO (Fig. 9g).

Allanite has not been observed in this study as a primary mineral in the samples from the western Mourne. The cores of secondary allanite-(Ce) crystals in association with epidote contain both Ce and Nd while the rims may contain Ce only (Fig. 9c, d). Strongly zoned allanite-(Ce) crystals up to 25 μm long also appear as inclusions trapped along annealed fractures in large crystals of quartz or feldspar. The epidote and particularly the allanite-(Ce) minerals in vein assemblages in the western Mourne contain up to 3 wt% MnO (Table 4), in marked contrast to the Mn-free allanite-(Ce) associated with primary granitic assemblages in the eastern Mourne. ΣREE is lower in vein allanite from the western Mourne than in either primary (G1) or secondary (G4) allanite-(Ce) (Fig. 9g) and Ce/La ratios are higher in vein allanite-(Ce) than in either G1 and G4 granites, which likely reflects a more oxidizing environment than the magmatic or post-magmatic environments in the eastern Mourne granites.

Rare karnasurtite-(Ce) $(\text{Ce},\text{La},\text{Th})(\text{Ti},\text{Nb})(\text{Al},\text{Fe}^{3+})(\text{Si},\text{P})_2\text{O}_7(\text{OH})_4 \cdot 3\text{H}_2\text{O}$ is identified on the basis of its platy habit with one good cleavage along which alteration has occurred (Fig. 8a), its greater water content as indicated by its total wt% relative to allanite-(Ce) (Table 4) and its contrasting stoichiometry relative to chevkinite $(\text{Ce},\text{La},\text{Ca},\text{Th})_4(\text{Fe}^{2+},\text{Mg})(\text{Fe}^{2+},\text{Ti},\text{Fe}^{2+})_2(\text{Ti},\text{Fe}^{2+})_2(\text{Si}_2\text{O}_7)_2\text{O}_8$. Chevkinite with a grain-size too fine for reliable analysis has tentatively been identified in association with radiating clusters of secondary allanite-(Ce) in G4 granite (Fig. 8d). Chevkinite-(Ce) was previously observed in G1 and G4 granites only (MacDonald *et al.* 2013), but karnasurtite-(Ce) has not previously been reported

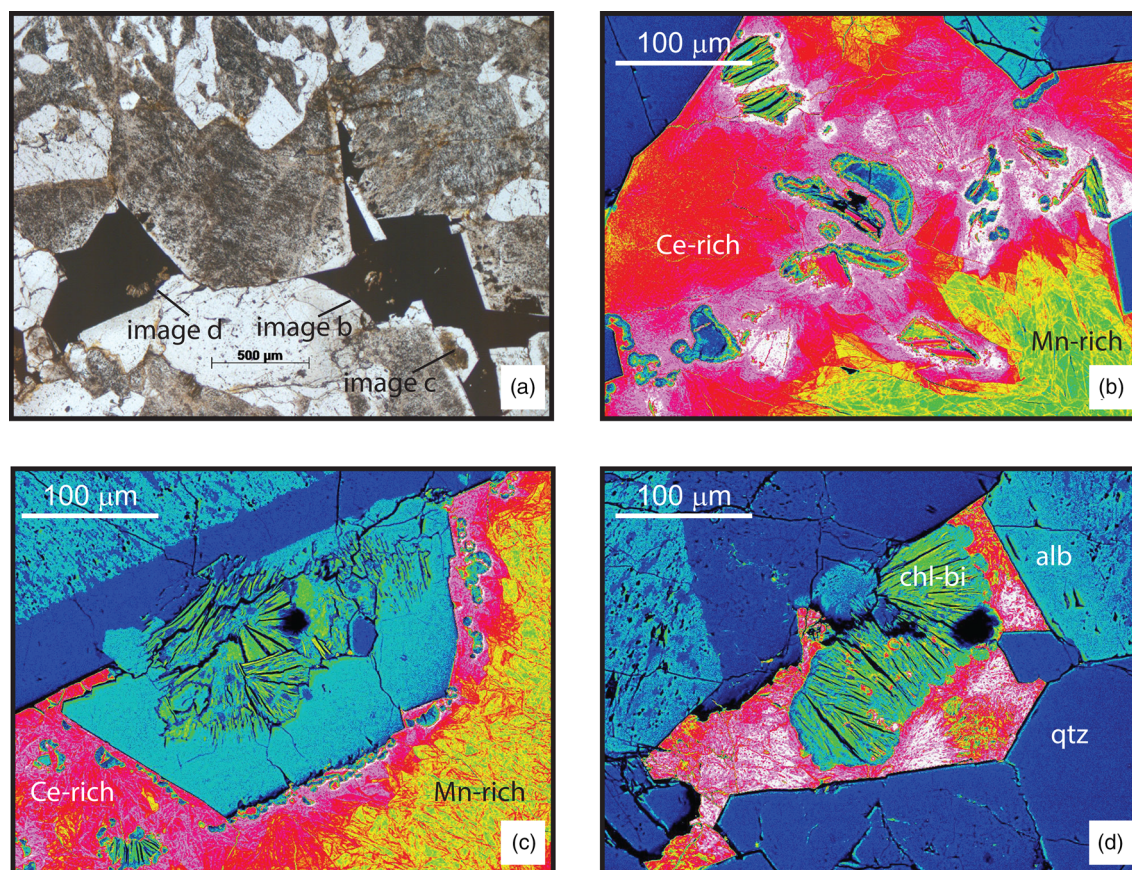


Fig. 6. Microphotograph (a) and false colour element maps (b–d) of infill of drusy cavity in G2 granite (sample WM2). Silicate minerals of the enclosing granitic assemblage are dark blue (quartz) and light blue (albite). Smaller chloritised biotite and chlorite crystals are included in the late-stage mineral assemblage infilling the cavity (green/blue). The secondary assemblage is dominated by an amorphous mass that varies from manganese-rich (bright green) to cerium-rich (white-pink) in composition.

in the literature for the Mourne Mountains, and neither mineral is a ubiquitous accessory phase. Karnasurtite-(Ce) is not commonly known as a mineral in metaluminous granites but it is a high-Th mineral characteristic of mineralization in peralkaline pegmatites of the Lovozero pluton (Ermolaeva *et al.* 2007).

Fe–Ti-oxide minerals, zircon and U-Th-minerals

Magnetite, ilmenite and rutile occur in both G2 and G4 granites, and in the outermost greisen of metasomatised G2 granite (Figs 8a, 10a). Primary magnetite in the granites is Ti-magnetite (mean 3.20 wt% TiO₂) with significant trace aluminium (average 1.95 wt% Al₂O₃) and variable manganese (up to 0.50 wt% MnO) content. In contrast, magnetite in the greisens contains lower titanium (mean 1.08 wt% TiO₂), aluminium (average 1.07 wt% Al₂O₃) and no manganese. Primary ilmenite occurs as lamellae within, and rims around, magnetite but is more resistant to local dissolution than the magnetite and there are significant differences in its chemistry between G2 and G4 granites. Manganese concentration is consistently high (mean 11.18 wt% MnO) and zinc is highly variable (up to 1.26 wt% ZnO) in ilmenite from the G2 granites whereas manganese is highly variable (mean 6.36 wt% MnO) and zinc is absent in ilmenite from the G4 granites. Rutile contains highly variable Nb₂O₅ (0–4.73 wt %) and WO₃ (0–2.88 wt%), regardless of whether it is located in unmetasomatised G2 granites or greisens.

There is an apparent association of the iron oxide minerals, particularly Ti-magnetite, with euhedral and zoned primary Hf-bearing zircon (Fig. 10a), and of both the Fe-oxides and zircon with a variety of Nb-Ti-, U-Th-, and REE-minerals (Fig. 10b). Rare micrographic intergrowth of cuneiform type occurs between magnetite-mantled zircon, which contains an assemblage of

various small (<10 µm) inclusions dominated by thorite and thorianite, with either quartz or biotite (Fig. 10b, c). A spongy texture forms where inclusions are dissolved from zircons (Fig. 10d). Primary zircon has highly variable composition and contains up to 4 wt% HfO₂, 3.4 wt% ThO₂, and 6.95 wt% UO₂. In some cases, the composition varies systematically as a function of zoning or leaching (Fig. 10e, f). Radially distributed fractures emanating from the crystal are filled with thorianite that has caused radiation damage in adjacent silicate minerals (Fig. 10e). The thorianite also crystallizes as small overgrowths on the margin of the zoned crystal, which has increasing Hf concentration and decreasing U and Th concentration from core to rim, with Th preferentially removed relative to U (Fig. 10f). The redistribution of Th therefore appears to be a very local post-magmatic process.

Subhedral zircon crystals in greisens are Hf-free and occur in association with monazite-(Ce) in a biotite pseudomorph (Fig. 8a). It is not clear from mineral textures whether they are the product of new crystallization with their morphology controlled by void space in spongy-textured biotite, or whether they are the corroded remains of primary zircon inclusions in biotite from which Hf and other chemical components have been removed. However, thorianite in the greisen contains up to 1.5 wt% As₂O₃, suggesting that metasomatic fluids may have been responsible for dissolution of zircon, such that primary zircon is corroded and re-precipitated.

Nb-Ti-Y(-REE) minerals

Primary mineral associations include: prismatic karnasurtite-(Ce) in association with magnetite and zoned zircon (Fig. 10a); euhedral fergusonite-(Y) Y(Nb,Ta)O₄ intergrown with tabular zircon (Fig. 10d) and zircon with spongy dissolution textures; and

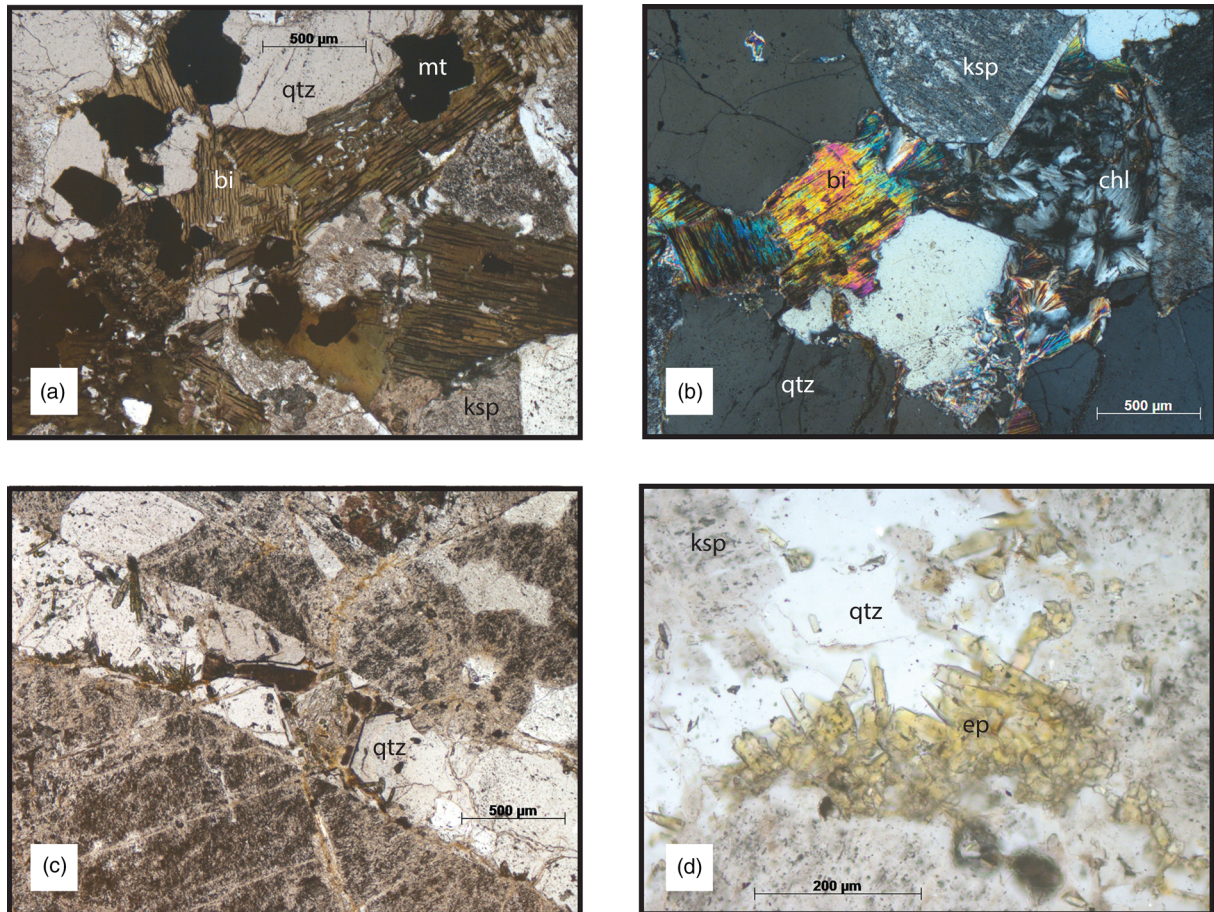


Fig. 7. Photomicrographs illustrating mineral assemblages in a shear zone through G4 granite at Gruggandoo (WM1). (a) Granite mineral assemblage showing an association between magnetite and biotite, sample WM1a, (b) Chlorite infill and alteration along grain boundaries, sample WM1a, (c) 1 mm wide quartz-epidote vein through G4 granite, sample WM1e, (d) Epidote crystal aggregate in vein, WM1e.

inclusions of various minerals in rare micrographic zircon mantled by magnetite that has associated aphanite $(\text{Nb,Ta,U,Fe,Mn})_4\text{O}_8$ (Fig. 10b) and rarely chernovite-(Y) $(\text{Ce,Y})\text{AsO}_4$. Inclusions in primary zircon crystals in pegmatite close to the contact between the G4 granite and the country rock comprise Dy-bearing yttriaite (Y_2O_3) and thorianite. In the micrographic intergrowth in G2 granite (Fig. 10b), euxenite-(Y) and xenotime-(Y) are inclusions in zircon, and aeschnite-(Y) is intergrown in magnetite mantles (Fig. 10c). Semi-quantitative analysis indicates that the Nb-rich phases aphanite and euxenite-(Y) sometimes contain trace tungsten. Aeschnite-(Y) in the Ti-magnetite mantles (Fig. 10c) has trace vanadium and significant tungsten (up to 8.67 wt% WO_3 , Table 5) in substitution for iron. The As-mineral chernovite-(Y), arsenic-bearing xenotime-(Y) and tungsten-bearing aphanite \pm euxenite-(Y) are primary minerals in G2 localities (samples EM1a, EM4a).

Secondary mineral textures are amorphous masses (Fig. 10g) with gradational compositions reflecting complex solid solution and/or admixtures, a replacement assemblage where euxenite-(Y) occurs in association with radiating sprays of allanite-(Ce) in a corroded biotite crystal (Fig. 10h), and an intimate association with anhedral rutile accompanying a monazite-(Ce)-dominated replacement assemblage in a spongy-textured biotite (Fig. 11a). The secondary infill in G4 granite (Fig. 10g) is amorphous but its core has variable euxenite-(Y) and aeschnite-(Y) compositions, while the outlying mineralized stringers are particularly U-rich and are considered to be metamict fergusonite-(Y) + euxenite-(Y) + uraninite \pm thorite. Small microveins in the G2 granite (Fig. 11b, c) also contain exceptionally hydrous, Ti-rich phases that are too small to be resolved quantitatively.

Fergusonite-(Y), euxenite-(Y) $(\text{Y,Ca,Ce,U,Th})(\text{Nb,Ti,Ta})_2\text{O}_6$ and aeschnite-(Y) $(\text{Y,Ca,Ce,Fe,Th})(\text{Ti,Nb})_2(\text{O,OH})_6$ in multiple primary (Fig. 10c) and secondary (Fig. 10g, h) parageneses were analysed using ESEM and EPMA (Table 5), and classified following the discussions of Ercit (2005), Ewing (1976) and Škoda and Novák (2007). These minerals have a wide range of compositions that encompass both Ti- and Nb-dominated chemical compositions (Fig. 12a, b) with no apparent correlation with paragenesis, host rocks or mineralogical context, except for some chemical evidence of alteration (Fig. 12c). A continuum of compositions and variable U/Th ratio relates to the inclusion of thorite in primary crystals, and leaching from primary crystals followed by enrichment in secondary phases. Therefore, some of the analysed compositions represent admixtures of euxenite-(Y) and aeschnite-(Y) with uraninite and thorite (Table 5, Fig. 12c). The mobility of Th decreases its reliability as a discriminator, but the aeschnite- and euxenite-group minerals in the Mourne Mountains Granites generally have lower Ta and Ca, but similar Y + ΣREE , compared to the REL-REE euxenite-subtype granite pegmatites (Fig. 12; cf Fig. 6 in Škoda and Novák 2007). The primary minerals consistently accommodate HREE whereas the HREE content of secondary minerals is highly variable (Table 5) in both the western and eastern Mournes granites.

REE phosphate and fluorocarbonate minerals

Subhedral primary monazite-(Ce) is up to 60 μm in size and occurs in association with magnetite/ilmenite (Fig. 11b), or as inclusions in magnetite (Fig. 11e) and karnasurtite-(Ce) (Fig. 10a) in samples of

Table 3. Representative major element compositions of mafic silicate minerals by ESEM analysis

Sample	Amphibole			Biotite					
	G1 EM5-2	G1 EM5-2	G1 EM5-2	G1 EM5-2	G1 EM5-2	G2 EM4a	G2 EM4a	EM2a_2	EM2a_2
SiO ₂	41.49	41.26	40.46	35.83	35.65	37.83	37.35	50.49	48.54
TiO ₂	1.05	1.04	1.16	3.65	3.64	2.76	1.89	0.00	0.82
Al ₂ O ₃	7.80	8.03	8.58	12.07	11.88	18.99	19.20	27.79	21.99
FeO	31.53	31.04	31.29	31.92	32.04	26.96	25.16	8.18	14.33
MnO	1.07	1.05	0.97	0.65	0.49	0.34	0.36	0.29	0.30
MgO	2.02	2.02	1.74	3.00	2.94	0.67	0.64	nd	nd
CaO	9.90	10.02	10.30	nd	nd	nd	nd	nd	nd
Na ₂ O	2.07	2.04	2.00	0.36	nd	nd	nd	nd	nd
K ₂ O	1.21	1.28	1.37	8.80	9.00	9.73	9.75	11.15	10.70
ClO	0.68	0.65	0.82	0.67	0.68	0.34	0.26	0.00	0.00
-O = Cl	0.15	0.15	0.18	0.15	0.15	0.08	0.06	0.00	0.00
Total	98.84	98.42	98.68	96.95	96.32	97.62	94.60	97.91	96.67

Sample	Biotite				Chlorite				
	EM2a_1	EM2a_1	EM2a_1	EM2a_1	G2 EM4a	G2 EM4a	EM2a_2	EM2a_2	EM2a_2
SiO ₂	45.40	47.38	48.83	47.66	46.92	46.02	35.60	33.66	39.14
TiO ₂	0.00	0.00	0.00	0.00	0.00	0.00	0.51	0.00	0.00
Al ₂ O ₃	29.75	31.59	32.01	32.45	11.49	13.95	17.12	18.67	19.49
As ₂ O ₃	1.24	1.19	0.00	0.00	0.00	0.00	0.00	0.00	0.00
FeO	4.37	3.97	3.67	2.80	26.30	27.03	27.08	31.73	21.86
MnO	nd	nd	nd	nd	0.00	0.00	0.48	0.47	0.33
MgO	nd	nd	nd	nd	0.39	0.44	0.76	0.00	0.73
CuO	nd	nd	nd	nd	0.00	0.00	2.68	1.99	1.90
CaO	nd	nd	nd	nd	0.40	0.33	0.00	0.00	0.00
Na ₂ O	nd	nd	nd	nd	0.84	0.84	0.00	0.00	0.00
K ₂ O	10.32	10.59	10.80	10.67	0.67	1.12	2.63	0.46	3.56
Total	91.08	94.72	95.31	93.59	86.99	89.73	86.86	86.97	87.00

Sample	Vein epidote			Replacement epidote			Zoned epidote			
	WM1e	WM1e	WM1e	WM1e	WM1e	WM1e	WM1e	WM1e	WM1e	WM1e
SiO ₂	38.83	38.58	38.98	38.27	38.14	37.44	38.43	39.73	38.49	38.49
TiO ₂	nd	nd	nd	nd	nd	nd	0.54	nd	nd	nd
Al ₂ O ₃	21.19	19.81	22.76	20.64	20.72	18.55	16.86	22.11	19.20	19.98
FeO	14.22	16.33	12.56	14.25	14.37	16.21	19.46	14.56	16.79	15.64
MnO	0.47	0.00	0.32	0.38	0.50	0.40	0.53	0.65	0.36	0.37
CaO	22.85	22.84	23.09	22.88	22.78	22.40	23.17	23.17	22.79	22.97
Total	97.57	97.55	97.71	96.43	96.51	95.00	99.00	100.22	97.64	97.45

nd, not detected by ESEM.

G2 and G4 granites. Primary monazite-(Ce) in both the G2 and G4 granites is Th-rich (mean 3.62 wt% ThO₂) and is Ce- and Nd-dominated (Table 5). Primary xenotime-(Y) occurs rarely as inclusions in zircon (Fig. 10c) in G2 granites and semi-quantitative analysis indicates that it contains significant Th ± trace As. Primary monazite-(Ce) inclusions in biotite are an order of magnitude larger than secondary monazite-(Ce) that occurs in association with bastnäsite-(Ce) ± cassiterite (Fig. 11a–d) in all the granites and/or with allanite-(Ce) in faults and shear zones in the western Mourne.

Secondary monazite-(Ce) contains significantly higher Th (mean 6.60 wt% ThO₂) than primary monazite-(Ce). Y + ΣREE is lower in secondary monazite-(Ce) (mean Y + ΣREE = 61.23 wt%) than in primary monazite-(Ce) (mean Y + ΣREE = 64.98 wt%) and the REE distribution is slightly different, with slightly higher La and lower MREE in secondary monazite-(Ce) (Table 5). The Th-enrichment in secondary monazite-(Ce) is likely to be a function of similar localized dissolution and reprecipitation phenomena that affected the distribution of Th around zircons (Fig. 10e, f). This is supported by mineral textures where, for example, secondary monazite-(Ce) has a dendritic habit and occurs in solution-widened cracks along cleavage in feldspars of G1 granites (sample EM5-2),

implying a low level of fluid infiltration in apparently primary granite samples. The large anhedral grain of cassiterite in Figure 11c and d partly infills magnetite pseudomorphs, while the monazite-(Ce) and bastnäsite-(Ce) preferentially precipitate in biotite with spongy dissolution textures, and is cross-cut by the localized veins of hydrous and amorphous Ti-rich mineralization.

Monazite-(Ce) also occurs together with bastnäsite-(Ce) as a secondary mineral in metasomatic replacement textures in greisens in G2 granite, where it is associated with arsenic-bearing minerals and small euhedral crystals of cassiterite ± rutile and zircon (Fig. 11f–h). The monazite-(Ce) – bastnäsite-(Ce) assemblage preferentially forms along the margins of quartz-cassiterite veins and does not occur within the veins themselves, illustrating the infiltration of fluids into the surrounding rock, particularly along crystal boundaries and cleavage planes (Fig. 11f). Secondary monazite-(Ce) in the greisens has significantly lower Th concentration than primary or secondary monazite-(Ce) in unmetasomatised granite (Table 5) and bastnäsite-(Ce) is Th-rich with more variable F concentration relative to secondary bastnäsite-(Ce) in granite.

An additional REE-phase is similar to chernovite-Y (Ce,Y) (AsO₄) in composition but has a large volatile component, variable

Table 4. Representative EPMA analyses of major element compositions of selected primary minerals: allanite-(Ce) (sample EM5-2, G1 granite) and karnasurtite-(Ce) (sample WM2, G4 granite)

	Allanite-(Ce)				Karnasurtite-(Ce)				
	Primary zoned* euhedral allanite				Euhedral		Corroded		
SiO ₂	34.41	31.96	34.01	34.04	19.28	18.73	20.48	19.31	19.10
TiO ₂	1.91	2.53	2.34	1.95	23.88	24.85	25.21	22.89	23.22
ThO ₂	0.52	1.60	1.46	0.70	10.62	9.96	9.69	7.75	9.19
UO ₂	b.d.	b.d.	0.10	0.08	0.49	0.57	0.57	0.40	0.49
Nb ₂ O ₅	b.d.	b.d.	b.d.	b.d.	1.03	1.00	1.01	1.09	1.18
Al ₂ O ₃ [†]	12.36	12.09	12.23	12.04	n.a.	n.a.	n.a.	n.a.	n.a.
Fe ₂ O ₃	15.79	16.51	17.23	16.81	12.46	12.57	11.80	12.56	13.26
La ₂ O ₃	6.60	6.26	5.00	6.18	4.28	4.25	4.28	5.72	5.03
Ce ₂ O ₃	12.21	10.78	11.08	13.15	5.21	5.71	5.81	8.36	7.41
Pr ₂ O ₃	1.15	1.00	1.04	1.39	0.91	0.71	0.93	1.23	0.92
Nd ₂ O ₃	0.00	3.23	b.d.	b.d.	3.14	3.17	3.40	4.07	3.74
Sm ₂ O ₃	0.66	0.27	0.53	0.57	0.50	0.60	0.62	0.77	0.50
Gd ₂ O ₃	0.28	0.24	0.19	b.d.	0.59	0.71	0.69	0.66	0.52
Dy ₂ O ₃	0.15	b.d.	0.20	0.05	b.d.	b.d.	b.d.	b.d.	b.d.
Ho ₂ O ₃	b.d.	b.d.	b.d.	b.d.	0.34	0.30	b.d.	b.d.	b.d.
Yb ₂ O ₃	b.d.	b.d.	b.d.	b.d.	0.17	b.d.	b.d.	0.17	b.d.
Y ₂ O ₃	0.50	0.30	0.38	0.51	0.33	0.38	0.38	0.45	0.47
MgO	0.71	0.57	0.40	0.71	n.a.	n.a.	n.a.	n.a.	n.a.
MnO	0.27	0.28	0.29	0.19	n.a.	n.a.	n.a.	n.a.	n.a.
CaO	9.62	8.77	8.26	9.43	1.51	1.29	1.45	1.53	1.52
P ₂ O ₅	b.d.	0.42	0.47	b.d.	0.51	0.56	0.54	0.38	0.50
ClO	0.02	0.02	0.03	b.d.	n.a.	n.a.	n.a.	n.a.	n.a.
-O = Cl	0.00	0.00	0.01	0.00					
Total	97.16	96.83	95.25	97.80	85.25	85.36	86.86	87.34	87.05
TREO	21.04	21.78	18.03	21.35	15.13	15.45	15.72	20.98	18.12

b.d., beneath detection limits; n.a., not analysed.

*Detailed analysis of chemical variation in zoned crystals is presented in Figure 9. Analysis tabulated above are for the crystal depicted in Figure 9b, f.

[†]Al₂O₃ was not included in analyses designed to determine REE concentrations accurately. However, EPMA analyses with semi-quantitative REE concentrations were used to determine that Al₂O₃ concentration is uniform regardless of the habit of karnasurtite-(Ce): mean = 1.08 wt%, standard deviation = 0.05 wt%.

Th concentration and affinity to bastnäsite-(Ce) in terms of F content and total oxide wt%. This mineral phase is not considered a new mineral species but more likely an intermixture, where bastnäsite-(Ce) has undergone replacement to chernovite-(Y).

As-minerals

Arsenic was observed in trace amounts substituting into inclusions in primary accessory minerals in unaltered G2 granite. In the eastern Mournes, As anomalies in the deep soil Tellus data are close to the G2 drusy granites and pegmatites and the G1 granite outcrops, and have an upper limit of 230 ppm (Fig. 2a). The overlapping, though differently oriented, As plume in Tellus stream sediment data has a similar order of enrichment over background levels as the soil data (Fig. 2b). At the southwestern extremity of the As anomaly at Pollaphuca (locality EM2a), As-minerals comprise 7.38 vol% of the >10 µm mineral fraction (Table 2) at the centre of a vein of metasomatic enrichment. Amphibole and biotite crystals have undergone progressive replacement from the margins to the centre of the mineralized zone (Fig. 13a–c) to an intermixture of scorodite, arseniosiderite (Fig. 13c–e, Table 6), and ultimately arsenopyrite (Fig. 13e). Multiple generations of intermediate phases with microbotryoidal and colloform habit (Fig. 13f) formed during partial replacement. The composition of the intermediate phases is often non-stoichiometric (Table 6) as a consequence of disequilibrium in the system. Complex solid solutions exist in the pharmacosiderite group and quantitative analysis indicates that the composition in Table 6 represents approximately 25% end member pharmacosiderite KFe₄(AsO₄)₃(OH)₄·6–7H₂O and 75% end member hydroxiumpharmacosiderite (H₃O)Fe₄(AsO₄)₃(OH)₄·4H₂O.

The highly porous microbotryoidal material was too fine-grained and porous for fully quantitative analysis but semi-quantitative EDX analysis revealed a highly variable composition, with significant strontium and bismuth. There appears to be extensive solid solution between end members of the crandallite group of minerals arsenogoyazite SrAl₃(AsO₄)₂(OH)₅·H₂O, arsenowaylandite BiAl₃(AsO₄)₂(OH)₆, arsenocrandallite CaAl₃(AsO₄)₂(OH)₅·H₂O and arsenoflorencite-(La): (La,Ce,Nd)(Al,Fe)₃(PO₄,AsO₄)₂(OH)₆. The crandallite group minerals formed in the early stages of replacement, such that the concentration of Ca and Al may reflect the composition of the replaced amphibole (hastingsite), and they are supplanted by pharmacosiderite + barahonaite + chenevixite, arseniosiderite + scorodite, and arsenopyrite as replacement progresses. The K and Ca in the phases pharmacosiderite KFe₄(AsO₄)₃(OH)₄·6–7H₂O and barahonaite (Ca,Cu,Fe,Al)₁₂Fe₂(AsO₄)(OH,Cl).nH₂O may also reflect components of pre-existing mineral phases that were locally re-precipitated.

Arsenoflorencite-(La) and chernovite-(Y) in the core of the metasomatic vein (Table 2) have LREE concentrations intermediate between niobate minerals and phosphate ± silicate REE minerals (Fig. 14). The rare occurrence of chernovite-(Y) is largely limited to the metasomatic rock, where it provides an alternative REE-mineral host to the secondary fluorocarbonate minerals and primary REE-bearing minerals of unmetasomatised granites. Thus it seems that the REE are present throughout the mineralization, substituting into As-rich minerals in the central part of the metasomatised zone and forming REE-phosphate minerals in the outer parts of the microveined metasomatised envelope. The distribution of Sn follows a similar trend, in that it substituted into a silica polymorph in the core of the mineralized zone and formed cassiterite at the margins. A highly variable Y-rich phase in the core

Table 5. Representative major element compositions of selected primary and secondary minerals from EMPA and ESEM: monazite-(Ce) (EM4a, G2 granite; EM2a/2, greisen), fergusonite-(Y) (EM4a, G2 granite; WM2, G4 granite), euxenite-(Y) (WM2, G4 granite), aeschynite-(Y) (EM4a, G2 granite) and amorphous admixtures of aeschynite-(Y) and thorite or uraninite (WM2, G4 granite)

	Monazite-(Ce)					Fergusonite-(Y)			
	P	p	s	s	m	EM4a		WM2	
SiO ₂	0.78	0.52	1.91	0.70	1.46	2.05	2.00	b.d.	b.d.
TiO ₂	n.a.	n.a.	n.a.	b.d.	b.d.	1.22	0.95	1.31	1.15
ThO ₂	3.48	2.86	7.44	4.19	1.03	6.17	5.62	4.29	4.48
UO ₂	0.32	0.24	0.31	0.38	b.d.	4.52	3.97	3.56	3.75
Nb ₂ O ₅	n.a.	n.a.	n.a.	b.d.	b.d.	42.75	43.89	43.82	45.93
Ta ₂ O ₅	n.a.	n.a.	n.a.	b.d.	b.d.	b.d.	b.d.	1.08	1.16
Fe ₂ O ₃	n.a.	n.a.	n.a.	n.a.	0.93	b.d.	b.d.	b.d.	b.d.
La ₂ O ₃	12.06	12.38	13.61	12.27	19.86	b.d.	b.d.	b.d.	b.d.
Ce ₂ O ₃	28.65	28.40	30.81	27.73	30.65	b.d.	b.d.	0.83	0.77
Pr ₂ O ₃	3.26	3.27	3.30	2.98	2.74	b.d.	b.d.	b.d.	0.39
Nd ₂ O ₃	13.50	13.86	10.20	12.27	9.22	1.95	1.97	1.86	1.83
Sm ₂ O ₃	3.12	3.05	1.64	2.99	1.38	b.d.	b.d.	1.19	1.32
Gd ₂ O ₃	1.80	1.85	0.53	1.79	0.89	13.00	12.14	2.20	2.28
Tb ₂ O ₃	b.d.	b.d.	b.d.	b.d.	b.d.	b.d.	b.d.	0.54	0.50
Dy ₂ O ₃	0.64	0.61	b.d.	0.73	b.d.	3.76	3.79	4.43	4.53
Ho ₂ O ₃	b.d.	0.48	0.51	0.36	0.39	b.d.	b.d.	1.19	1.06
Er ₂ O ₃	b.d.	0.22	b.d.	b.d.	b.d.	b.d.	b.d.	3.34	3.34
Yb ₂ O ₃	b.d.	b.d.	b.d.	b.d.	b.d.	b.d.	b.d.	2.17	2.23
Y ₂ O ₃	2.18	1.90	b.d.	1.66	b.d.	22.88	22.90	25.88	25.58
CaO	0.29	0.27	0.27	0.54	0.12	0.79	0.90	0.70	0.81
P ₂ O ₅	28.41	28.39	27.97	30.04	31.33	b.d.	b.d.	b.d.	b.d.
Total	98.49	98.30	98.50	98.64	100.00	99.08	98.14	98.39	101.11
TREO	63.03	64.12	60.60	61.13	65.13	18.71	17.90	17.75	18.24

	Euxenite-(Y)	Ferro-aeschynite-(Y)	Niobo-aeschynite-(Y)	Admixtures				
SiO ₂	1.48	3.21	3.49	0.00	1.28	5.68	4.37	b.d.
TiO ₂	47.39	35.80	34.81	35.22	30.95	3.46	3.24	0.35
ThO ₂	b.d.	4.69	4.84	3.74	3.77	18.13	4.79	6.58
UO ₂	b.d.	b.d.	b.d.	0.00	8.09	7.79	43.40	10.65
Nb ₂ O ₅	b.d.	b.d.	b.d.	7.36	4.33	25.51	17.86	33.86
Ta ₂ O ₅	b.d.	b.d.	b.d.	b.d.	b.d.	4.21	4.75	3.43
Fe ₂ O ₃	0.71	3.47	3.80	0.00	0.90	6.01	7.59	10.54
La ₂ O ₃	b.d.	b.d.	b.d.	b.d.	b.d.	b.d.	b.d.	b.d.
Ce ₂ O ₃	b.d.	b.d.	b.d.	6.11	4.56	b.d.	b.d.	0.47
Pr ₂ O ₃	b.d.	b.d.	b.d.	b.d.	b.d.	b.d.	b.d.	b.d.
Nd ₂ O ₃	1.80	1.87	1.93	7.99	5.46	b.d.	0.22	1.14
Sm ₂ O ₃	b.d.	b.d.	b.d.	b.d.	b.d.	b.d.	b.d.	0.91
Gd ₂ O ₃	12.03	10.09	11.69	b.d.	b.d.	0.22	b.d.	1.11
Tb ₂ O ₃	b.d.	b.d.	b.d.	b.d.	b.d.	b.d.	b.d.	b.d.
Dy ₂ O ₃	4.23	b.d.	b.d.	b.d.	b.d.	b.d.	b.d.	1.79
Ho ₂ O ₃	b.d.	b.d.	b.d.	b.d.	b.d.	b.d.	b.d.	0.75
Er ₂ O ₃	3.18	2.96	b.d.	b.d.	b.d.	b.d.	b.d.	0.85
Yb ₂ O ₃	3.07	b.d.	b.d.	b.d.	b.d.	b.d.	b.d.	1.41
Y ₂ O ₃	25.13	15.84	14.49	13.56	11.82	b.d.	b.d.	3.79
CaO	b.d.	b.d.	b.d.	b.d.	b.d.	0.43	0.59	0.39
P ₂ O ₅	b.d.	b.d.	b.d.	b.d.	b.d.	0.56	b.d.	b.d.
WO ₃	b.d.	5.80	4.52	8.67	6.92	b.d.	b.d.	b.d.
Total	99.02	83.74	79.57	82.66	78.07	72.01	86.81	78.03
TREO	24.31	14.92	13.62	14.10	10.02	0.22	0.22	8.44

p, primary; s, secondary monazite-(Ce); m, monazite-(Ce) in metasomatic replacement texture in greisen. n.a., not analysed; b.d., beneath detection limit.

of the metasomatism was located as a potential HREE-rich replacement of euxenite-(Y) and aeschynite-(Y), or karnasurtite-(Ce). It can be postulated that REE and Sn are only locally remobilized and their concentration is fairly constant throughout the mineralization. The barahonaite and chenevixite $\text{Cu}_2\text{Fe}_2(\text{AsO}_4)_2(\text{OH})_4$ illustrate that Cu is an important cation that is introduced by the metasomatising fluid. Bromine and chlorine both replace the hydroxyl anion in several of the mineral species (for example, chenevixite, scorodite, and barahonaite; Table 6). Coupled with the abundance of F-rich topaz in the core of the mineralized zone

(8.63 vol%, Table 2), this suggests that the metasomatic fluids were very halide-rich.

Discussion

Overview of the mineralogical sources of geochemical anomalies in the Mourne Mountains

The four major patterns of chemical anomaly that were identified in the Tellus geochemical (stream and deep soil) data correlate with the

Table 6. Representative major element compositions of hydrous arsenic-rich minerals, by ESEM analysis

wt%	Arsenosiderite				n-s chenevixite				
SiO ₂	0.71	0.74	0.73	0.60	0.00	0.62	0.54	0.58	
Al ₂ O ₃	0.00	0.00	0.00	0.67	0.00	0.00	0.00	0.68	
Fe ₂ O ₃	31.98	31.38	31.67	45.00	44.20	42.39	44.90	43.01	
As ₂ O ₃	38.09	37.68	39.14	18.15	18.50	18.41	17.42	17.76	
CuO	0.61	0.50	0.00	3.41	3.10	3.15	3.54	3.72	
CaO	13.67	13.81	13.92	0.70	0.71	1.82	nd	nd	
K ₂ O	nd	nd	nd	nd	nd	nd	nd	nd	
BrO	nd	nd	nd	nd	1.36	0.97	1.02	nd	
ClO	nd	nd	nd	nd	nd	nd	nd	nd	
-O = Br	nd	nd	nd	nd	0.14	0.10	0.10	nd	
-O = Cl	nd	nd	nd	nd	nd	nd	nd	nd	
Total	85.06	84.11	85.46	68.52	67.73	67.27	67.30	65.75	

wt%	Scorodite			n-s pharmacosiderite			n-s barahonaite	
SiO ₂	1.25	1.09	1.45	1.20	0.77	0.75	0.76	0.90
Al ₂ O ₃	0.00	0.99	0.00	0.00	0.00	0.00	0.53	0.49
Fe ₂ O ₃	31.24	31.70	31.94	42.61	42.90	43.32	45.82	45.86
As ₂ O ₃	39.26	42.23	40.65	37.09	38.79	38.72	19.14	19.91
CuO	nd	nd	nd	1.13	0.74	0.76	2.06	1.97
CaO	nd	nd	nd	1.56	0.00	0.00	0.65	0.65
K ₂ O	nd	nd	nd	1.28	1.84	1.17	nd	nd
BrO	2.55	nd	2.52	nd	nd	nd	nd	nd
ClO	nd	nd	nd	nd	nd	nd	0.41	0.40
-O = Br	0.26	nd	0.25	nd	nd	nd	nd	nd
-O = Cl	nd	nd	nd	nd	nd	nd	0.09	0.09
Total	74.04	76.00	76.30	84.87	85.04	84.72	69.28	70.09

n-s, non-stoichiometric; nd, not detected by ESEM analysis.

mineralogical observations in the bedrock samples. This corroborates the findings of Steiner (2019, 2018) that regional geochemical datasets can not only define anomalous areas and enrichments of incompatible elements of economic interest, but provide understanding of geological setting and definition of ore deposit styles. We describe the ore deposit styles as four anomaly types.

Anomaly type 1 comprised Th, REE and Nb (Fig. 1) enrichments associated with G1 and G2 granites in the eastern Mourne. These correlate with the primary allanite-(Ce)+mafic silicate or the primary niobates+zircon+Fe–Ti oxide mineral associations. Variable textures in the zircon are indicative of primary crystallization, dissolution, re-crystallization and overgrowths (Alekseev and Alekseev 2020). Fergusonite-(Y) was observed intergrown with zircon in bedrock samples (Fig. 10d) in a primary magmatic association, where zircon had a spongy texture that probably resulted from dissolution of thorianite inclusions akin to those depicted in Figure 10c. However, primary magmatic fergusonite-(Y) was rare and the extensive soil Nb anomaly in the eastern Mourne is attributed to minerals in which Nb ± Ta is chemically coupled to Ti: aeschynite-(Y) and fergusonite-(Y) as primary inclusions in zircon, primary euhedral crystals, and secondary mineralization infilling cavities (e.g. Figs 10c, g and h). Primary karnasurtite is associated with primary monazite-(Ce) (Fig. 10a) and xenotime inclusions (Fig. 10c), and secondary euxenite-(Y) and aeschynite-(Y) occur in association with secondary allanite-(Ce) ± cassiterite (Figs 10h, 11c).

The primary niobate minerals such as euxenite-(Y) and fergusonite-(Y) have an extremely high Nb/Ta ratio: for the euxenite-(Y) analyses in Table 5, mol Nb/Ta = 79 and 69. Admixtures of niobate minerals in replacement assemblages (Table 5) have mol Nb/Ta ratios in the range of 6.6–17.3. Influences on Nb/Ta ratio include the crustal v. mantle source region, the extent and temperature of fractionation and the magmatic-hydrothermal transition, and the presence of critical ligands such as F (Chevychev *et al.* 2005; Ballouard *et al.* 2016;

Stepanov *et al.* 2016). The high relative Nb concentration in the Mourne Mountains granitic magmatic-fluid system (primary and secondary mineralization) likely reflects the mantle source region and the preferential incorporation of Nb over Ta in accessory phases in dominantly subaluminous granitic systems, which results in a late-stage fluid with lower Nb/Ta ratio despite the lower solubility of Ta (Green 1995; Linnen and Keppler 1997; Chevychev *et al.* 2005; Ballouard *et al.* 2016). Although Hf-bearing zircon with associated REE can be indicative of productive ore-magmatic systems (Alekseev and Alekseev 2020), a high Nb/Ta ratio, such as for the Mourne Mountains, would plot in the ‘barren’ field of peraluminous granites of Ballouard *et al.* (2020). Whether the plot is representative for granites that are not peraluminous is unknown.

Monazite-(Ce) and allanite-(Ce) contain only LREE (La, Ce and Nd), whereas there is substitution of Gd, Dy and Er for Y in aeschynite-(Y) and euxenite-(Y) (Tables 5 and 6; Fig. 13). The REE in G2 niobates is dominantly hosted by fergusonite-(Y) whereas the REE in G4 niobates is dominantly hosted by aeschynite-(Y). The niobate minerals, particularly in G2 granites, contain nearly as much Dy as xenotime-(Y), which is a potentially economic source of HREE in carbonatites (Fig. 14). The association of Ce anomalies and REE, Nb ± Ta, Th ± U enrichments in the roof zones of the eastern Mourne granites that contain zoned (Fig. 10e, f) and primary (Fig. 10a) euhedral crystals, and primary inclusions and intergrowths (Fig. 10b, c) demonstrate that magmatic recharge of evolved magmas and eutectic crystallization were important processes that concentrated the critical metals.

Chemical components (particularly Th) have been subject to some local leaching and re-precipitation (e.g. Figs 10e, f and 12c), where bastnäsite-(Ce) is associated with secondary monazite-(Ce) (Fig. 11a–c). The higher Th content of secondary monazite-(Ce) is consistent with the localization of remobilization textures (Liu *et al.* 2022). Regardless of context, monazite-(Ce) and bastnäsite-(Ce) have a limited compositional range and display characteristic extreme LREE enrichment (Fig. 14). Secondary cassiterite is

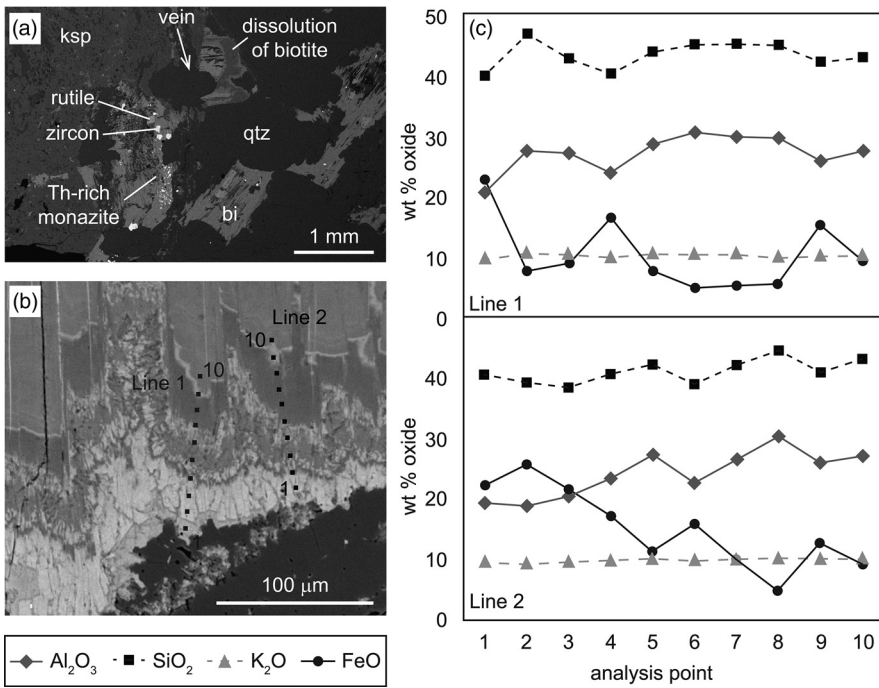


Fig. 8. BSE images of (a) biotite crystals on the margins of a quartz vein undergoing dissolution, with infill by precipitation of high atomic mass minerals, including Ti-magnetite, zircon, cassiterite and monazite-(Ce), and (b) the location of analytical transects across the top right biotite crystal in (a), (c) shows the composition of biotite along the analytical transects, expressed as wt % oxide.

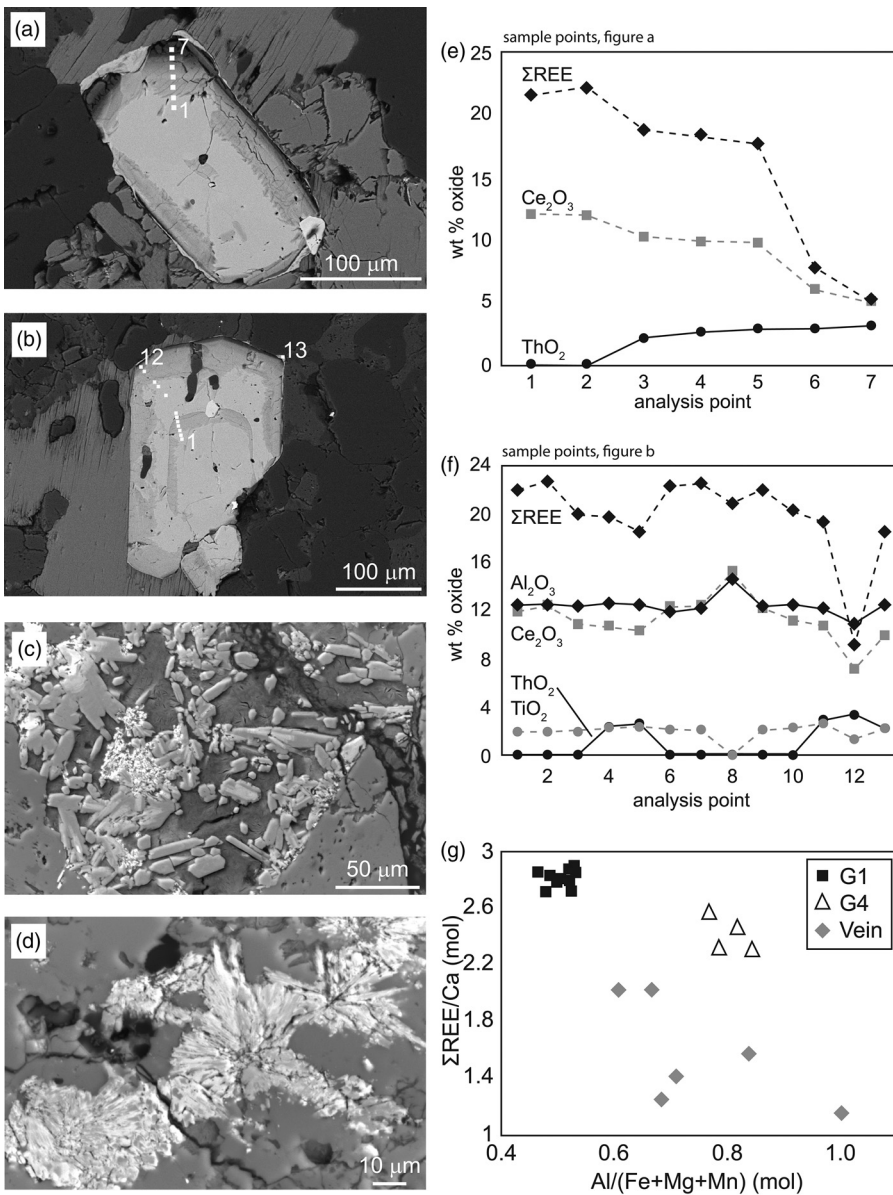


Fig. 9. BSE images of zoning in primary magmatic allanite-(Ce) in the G1 granite (a, b, sample EM5-2) and 2 generations of secondary allanite-(Ce) growth in G4 granite (c, d, sample WM1e). The zones in magmatic allanite-(Ce) crystals where examined in detail using quantitative ESEM analysis. REE abundance is expressed as Σ REE and Ce concentration (e, f), for which analytical confidence was determined using EPMA analysis (Table 4). Chemical variation between allanite-(Ce) populations (g) in G1 (sample EM5-2), G4 (sample WM2) and vein allanite-(Ce) (WM1e) is examined using covariation of mol ratios Σ REE/Ca and $Al/(Fe^{2+} + Mg + Mn)$ by ESEM analysis.

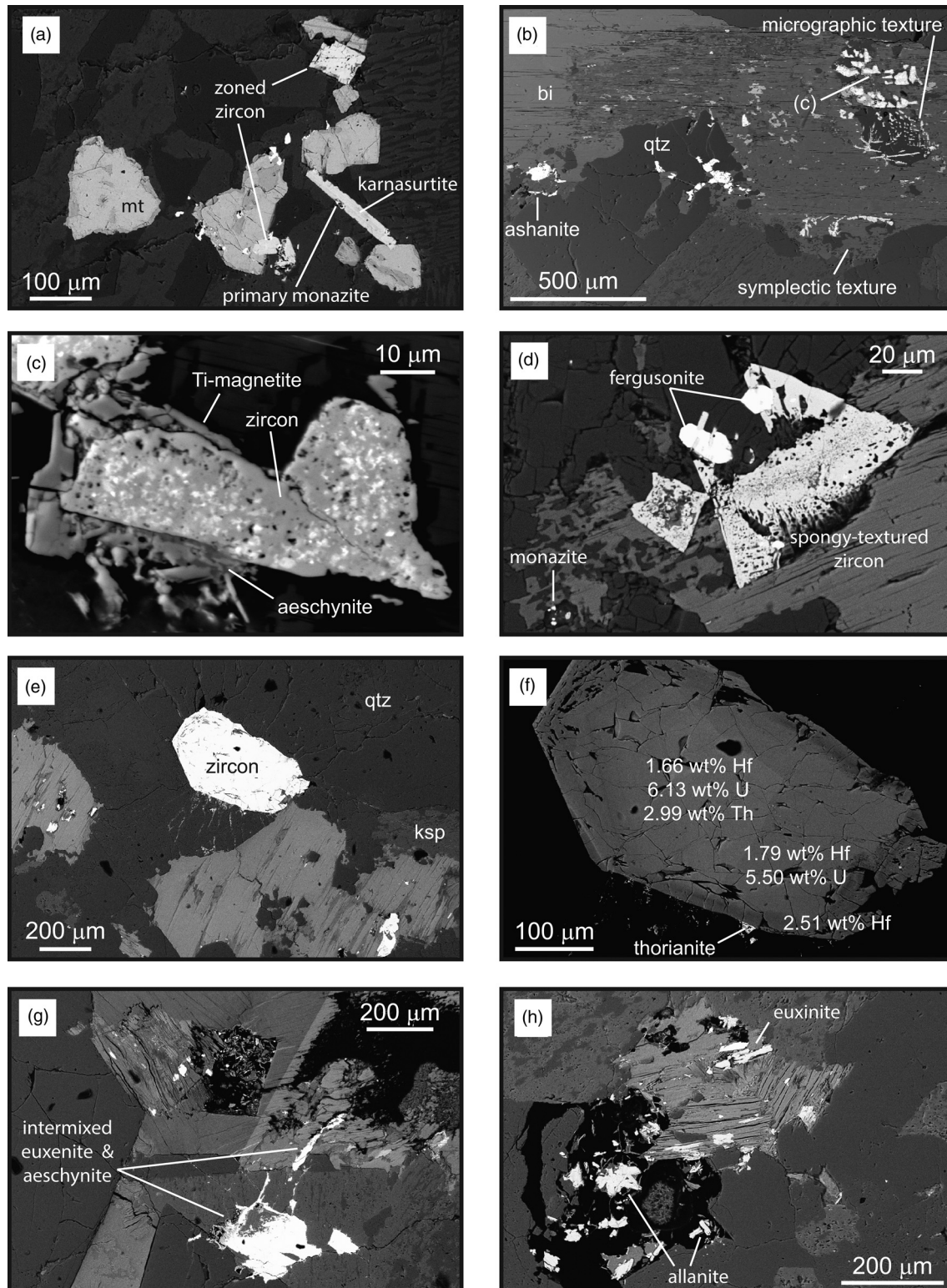


Fig. 10. BSE images showing the occurrence of (a) magnetite with ilmenite lamellae and rims in association with zoned zircon, prismatic karnasurtite-(Ce) undergoing alteration to ferriallanite-(Ce) and monazite-(Ce) inclusions (sample WM2), (b) biotite-quartz symplectic texture and micrographic texture between a zircon-rich mineral assemblage and biotite + quartz (EM1a), (c) detail of a zircon crystal from figure 9a containing a variety of inclusions, mantled by magnetite with aeschynite-(Y) intergrowth (EM1a), (d) euhedral fergusonite-(Y) with tabular zircon intergrowths (sample EM1a), (e) euhedral fergusonite-(Y) associated with spongy-textured zircon and primary monazite-(Ce) inclusions (sample EM1a), (f) compositional zoning related to depletion of Th, U and Hf, (wt% element) in the same crystal, (g) amorphous infill/replacement structure including euxenite-(Y) and aeschynite-(Y) compositions (sample WM2), and (h) allanite-(Ce) and euxenite-(Y) replacement mineralization (sample WM2).

associated with the local re-precipitation of magmatic minerals (Fig. 12b, c). This suggests that Sn resided in late-stage magmatic fluids that were trapped within the crystallizing granite, perhaps because of HCl-rich and F-depleted compositions of magmatic

fluids that were exsolved late (Hu *et al.* 2009; Schmidt *et al.* 2020; Zhao *et al.* 2022).

Anomaly type 2 comprises enrichments in As (Fig. 2), Sn, REE and Y, where the largest positive arsenic anomaly in stream

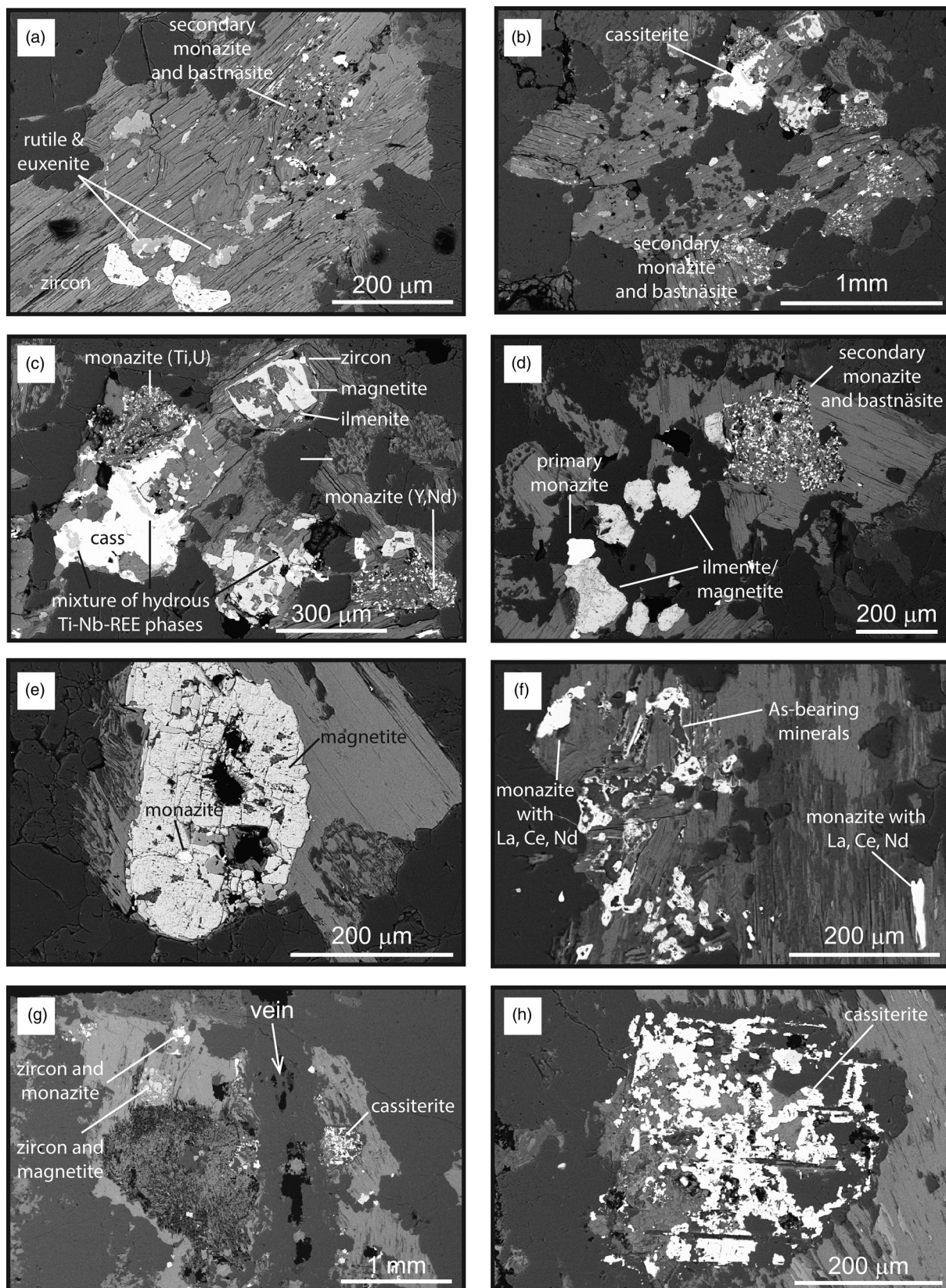


Fig. 11. BSE images illustrating the occurrence of monazite-(Ce) and bastnäsite-(Ce) in samples EM4a (a–e), EM2a_2 (f) and EM2a_3 (g, h). Euxenite-(Y) is intergrown with rutile (a). Fine-grained monazite-(Ce) of variable composition and bastnäsite-(Ce) are secondary (a–d) and occur in biotite with zircon and cassiterite (c, f–h). Primary monazite-(Ce) is an order of magnitude larger than secondary magnetite and occurs in association with magnetite (b, e). Replacement cassiterite can be massive in association with localized remobilization structures (c, d) or controlled by the crystallographic structure of the pseudomorphed mineral on the margin of veins (h).

sediments appears to emanate from zoned metasomatism at sample location EM2 (Pollaphuca) in the eastern Mourne Mountains. Host silicate minerals have a characteristic trace element signature in

metasomatised samples of Sn and In (in silica polymorphs), Mn and Cu (in chlorite), As (in biotite), and F (in topaz). Dissolution reduced the chlorine concentration in biotite such that overgrowths

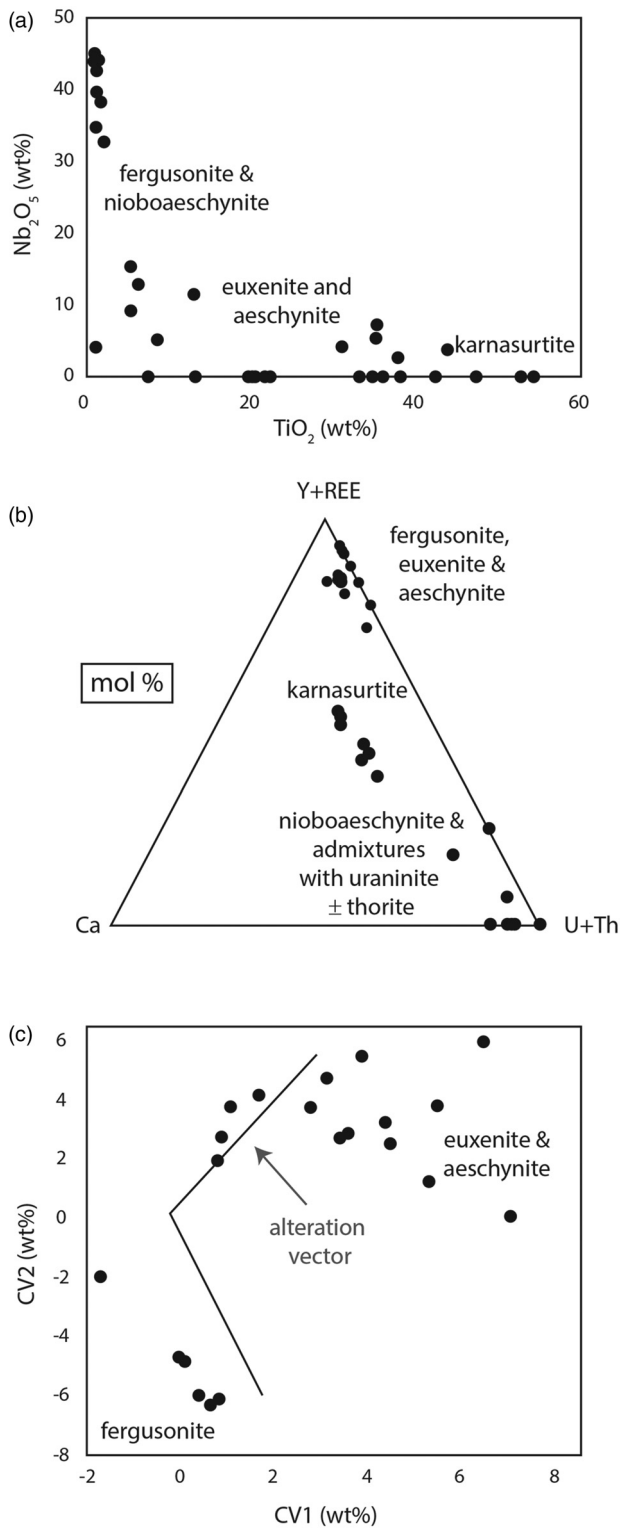


Fig. 12. Compositional variation in the Nb-Ti oxide mineral groups, and admixtures of Nb-Ti oxide minerals with U-Th minerals and amorphous masses, as wt% oxide (a), mol% (b), and using the canonical variables and classification boundaries (c) of Ercit (2005). Also shown is the alteration vector described by Ercit (2005), for hydration and addition of Si, Al, K, Ba and Sr, which is important for the infill mineralization depicted in Figure 10g, h.

on biotite were potassium-enriched. The F/Cl ratio appears to be elevated relative to anomaly type 1.

As minerals contain bromine and LREE concentrations intermediate between other REE minerals (Fig. 14). The chemistry of all the mineral groups indicates that As and Cu metals were added by

potassic and halide-rich fluids, and that Sn and REE were redistributed during the progressive replacement (Fig. 13) of mafic silicate minerals and feldspars. The source of the indium, occurring together with tin as impurities in silica polymorph(s), is enigmatic but it may have been released from the mafic minerals that were replaced (Adam and Green 2006). The characteristic chemical signature is in marked contrast to all the other anomalies and indicates a more F-rich and voluminous fluid transported a significantly different metal budget.

It appears that with extensive fluid migration through granite, the primary magmatic REE-Nb mineralization in anomaly type 1 is progressively replaced with monazite-(Ce) + bastnäsite-(Ce), and then arsenoflorencite-(La) + chernovite-(Y). Evidence for the source of the As-W-bearing metasomatising fluids comprises primary chernovite-(Y), arsenic-bearing xenotime and tungsten-bearing aphanite ± fergusonite-(Y) or euxenite-(Y) in G2 localities that were not affected by metasomatism, which suggests affinity with the granite magmas. If As preferentially partitions into late-stage magmatic fluids, then the progressive nature of metasomatism and the apparent linearity of the As enrichment in the Mourmes (Fig. 2a) in the Tellus data suggest that multiple pulses of magmatic fluids derived from granitic intrusions were concentrated along linear structural features that penetrated through the granite laccolith. Although there is a possibility of down-slope creep from a point source, fluid-focusing is needed for the extent of metasomatism observed in the samples.

The mineralogical evidence in anomaly type 2 indicates that petrogenetic process is a controlling factor in formation of the point source to the arsenic plume in Figure 2b. The association of petrogenetic process with a high concentration of deleterious elements that are mobile in soil and stream sediments can be factored into minerals systems approaches to exploration (e.g. Banks *et al.* 2019, 2020) and the increasingly important responsible sourcing agenda (Wall *et al.* 2017; Kügerl *et al.* 2023; Stephenson *et al.* 2023).

Anomaly type 3 comprises enigmatic, isolated and scattered areas where manganese and cerium concentration rise above background levels (Fig. 1c). Drusy granite infill in sample WM2 contains a very clear association between Ce and Mn. The mineralization (Fig. 6) has highly variable composition from a manganese-rich to cerium-rich hydrous amorphous mass, with accompanying Ca, Pb, Ba, As, S, Br and Cl. The low concentration of As and the Mn enrichment have affinity to the magmatic host rocks of Anomaly type 1 and the metasomatic fluids of Anomaly type 2, respectively. The most notable coupling between Ce and Mn in Anomaly type 3 has been observed in many other geological environments, since Mn and Ce are recognized as having similar redox characteristics and a range of common mechanisms for oxidation in a wide range of marine environments (Moffett 1994). For example, Mn-rich mineral overgrowths and late fracture fill are associated with secondary fluids from a magmatic source that produce Ce-dominated daughter minerals (Costanzo *et al.* 2006), as fracture fill relating to remobilization of formation/hydrothermal fluids (Yu *et al.* 2017), while ocean floor Mn nodules have Mn and REE in concentrations that have positive correlations with Fe content (Glasby *et al.* 1987; Godfrey *et al.* 1997). The unifying characteristic is that the Ce anomalies are associated with oxidation of the system. In the case of the Mourne Mountains, speciation to Ce⁴⁺ occasionally creates positive anomalies in magmatic processes such as magmatic recharge (analysis point 8; Fig. 9f). Where magmas and fluids coexist, speciation can drive partitioning of Ce into fluids that are more oxidizing than magmas (Pourret *et al.* 2008; Yu *et al.* 2017).

It is possible that the infilled drusy cavities of Anomaly type 3 represent a near-source stage in the physical and chemical evolution of fluid expelled from magma, intermediate between the very local remobilization of REE and Th with re-precipitation of granitic

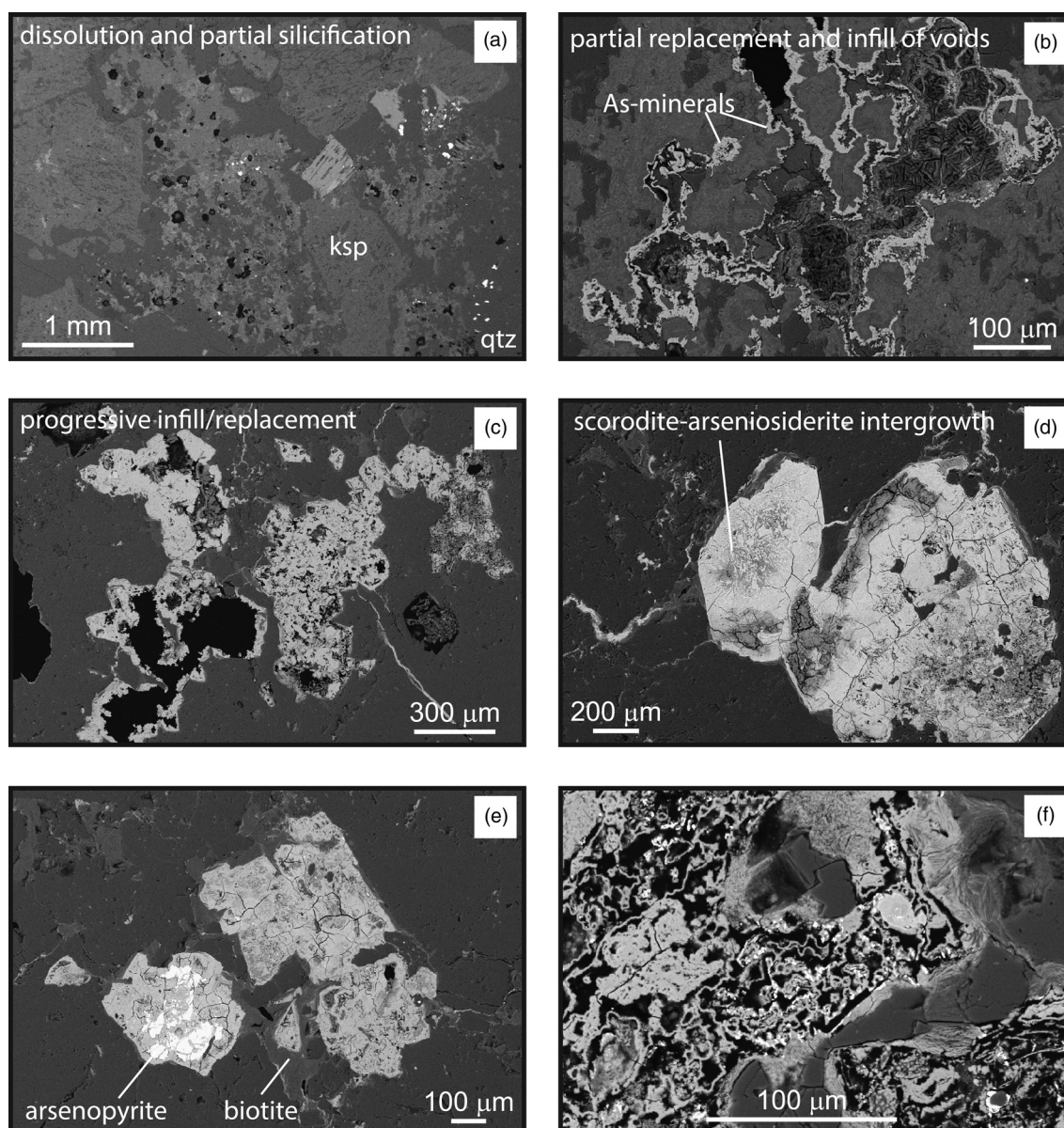


Fig. 13. BSE images showing progressive replacement of mafic silicate minerals in G2 granite by As-rich minerals at Pollaphuca. (a) Spongy dissolution and silicification of amphibole, with replacement of biotite by chlorite, sample EM2a-3, (b) Infiltration of fluids along grain boundaries and precipitation of As-minerals in voids and along grain boundaries, sample EM2a-2, (c) Replacement of crystals from grain boundaries to the centre of crystals, sample EM2a_1, (d) Development of an arseniosiderite-siderite intergrowth in a crystal undergoing complete replacement, sample EM2a_1, (e) Further organization and replacement of a crystal by arsenopyrite, sample EM2a_1, (f) Detail of botryoidal/colloform highly porous infill (including crandallite group minerals) with some acicular overgrowths on remnant minerals typical of partial replacement, sample EM2a_1.

accessory minerals by very small fluid volumes (Anomaly type 1) and the focusing of large volumes of fluid probably along some structural feature (Anomaly type 2). The implications of this hypothesis are that either Ce + Mn were rapidly removed from granite-sourced fluid that evolved to become very As-enriched, or that fluids of different composition and volume separated from the granitic magma by different mechanisms. Regardless, it appears that the critical metals associated with the small anomalies of Anomaly type 3 were remobilized and concentrated into cavities in granite host rock. It appears that the percolation of fluids occurred over small distances, such that remobilization was most likely by magmatic fluids. However the possibility exists, that other fluids mixed with magmatic waters using a more extensive network of fluid flow paths, where transient fracturing was associated with the magmatic-hydrothermal transition (Gillis and Roberts 1999).

Anomaly type 4 is spatially associated with observed tectonic lineaments and is most pronounced in the western Mourne. Allanite-(Ce) and monazite-(Ce) that was located in the bedrock

samples had small grain-sizes and occurred dominantly in chlorite-rich pockets along grain boundaries and as mineral infill of void spaces, such that the mineralogical context is clearly secondary. Monazite-(Ce) was not observed in association with bastnäsite-(Ce) or cassiterite. The lower REE concentrations, more variable composition (Figs 9g, 14) and higher Ce/La ratio show that vein allanite-(Ce) of Anomaly type 4 has a very different nature to allanite-(Ce) in Anomaly types 1–3, likely related to a more oxidized environment (Glasby *et al.* 1987; Pourret *et al.* 2008). Given the association of the mineralization with post-intrusion tectonic lineaments, this opens the possibility of an influx of mineralizing fluids that do not have a magmatic origin. The interpretation is supported by the diversity and highly variable nature of heavy mineral concentrates (Moles and Tindle 2011, 2012; Moore *et al.* 2016), but fluid inclusion and stable isotope studies have indicated that the Mourne Granite complex beneath the roof zone has been unaffected by regional-scale fluid influxes (McCormick *et al.* 1993; Conliffe and Feely 2010). The implication

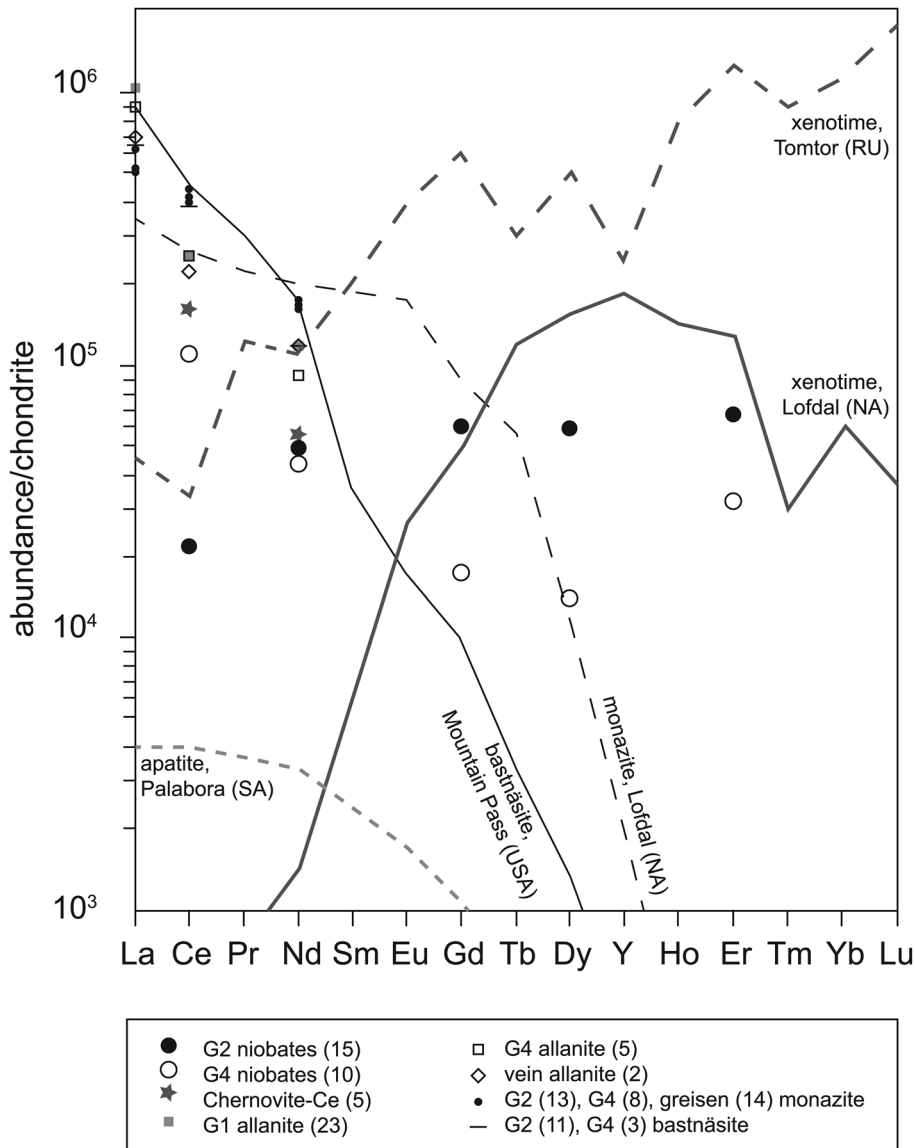


Fig. 14. Comparison of mean REE concentration in REE and Nb-Ti minerals (figure in parentheses denotes *n*, the number of analyses used in the average calculation) in the Mourne Mountains granites with representative REE-enriched mineral deposits worldwide. The niobates included in the average calculations are karnasurtite-(Ce), aeschynite-(Y), euxenite-(Y), and fergusonite-(Y). Normalized using the data of Sun and McDonough (1989). Mineral data for carbonatites from Chakhmouradian and Wall (2012), Hornig-Kjarsgaard (1998); Wall *et al.* (2008).

is that fluids may have a more local meteoric component (Pourret *et al.* 2008).

Petrogenesis of rare-metal enrichments in the Mourne Mountains

The four anomaly types encompass a multi-stage petrogenetic model for the concentration of REE, Nb, Th and associated elements (Fig. 15) whereby:

- (1) Critical metals are concentrated during late-stage and eutectic magmatic crystallization of a volatile-rich magma to generate drusy granites and pegmatites;
- (2) Late-stage magmas evolve magmatic fluids that transport critical metals, and ascend to metasomatise pre-existing granitic rocks \pm infill drusy cavities;
- (3) Subsequently, fluids remobilize and transport critical metals to greater concentration along fluid-flow channels, such as tectonic lineaments.

It is not suggested that the mineralization in the Mourne Mountains granites has economic potential but the combination of processes observed in this multi-stage model is representative of the petrogenesis of many economic igneous deposits of REE, which have accounted for >50% of global REE production between the

1960s and 1995 (Chakhmouradian and Zaitsev 2012). The majority of igneous rocks with economic REE concentrations are carbonatites, peralkaline felsic rocks and, to a lesser extent, pegmatites associated with some sub- to met-aluminous granites. A common feature for these occurrences is a magmatic source region enriched in incompatible elements, which undergoes decompression melting often in intracontinental, anorogenic, or extensional settings. The combination of a parental magma from an enriched mantle source, extensive fractionation, element mobility at the magmatic-hydrothermal transition, and subsequent remobilization (Fig. 15) is a typical route to enrichment of critical metals in granites (Ballouard *et al.* 2016; Smith *et al.* 2016; Honour *et al.* 2018; Kaeter *et al.* 2018; Shaw *et al.* 2022). The diversity of primary Y/HREE-bearing minerals in the early peralkaline to metaluminous granites, drusy granites and pegmatites (G1 and G2) of the Mourne Mountains is consistent with extensive fractionation from mafic parental magmas, formed due to upwelling of mantle beneath an intact continental lithosphere (Meighan *et al.* 1984; Kent and Fitton 2000; Stevenson and Bennett 2011).

The primary magmatic intergrowth of REE- and Nb-bearing minerals with silicate minerals under eutectic crystallization conditions in drusy G2 roof zone granites (e.g. EM1, Diamond Rocks) is of particular interest when the accessory mineral assemblage in drusy cavities is considered. The distribution of the drusy cavities demonstrates that the F-rich late-stage magmatic

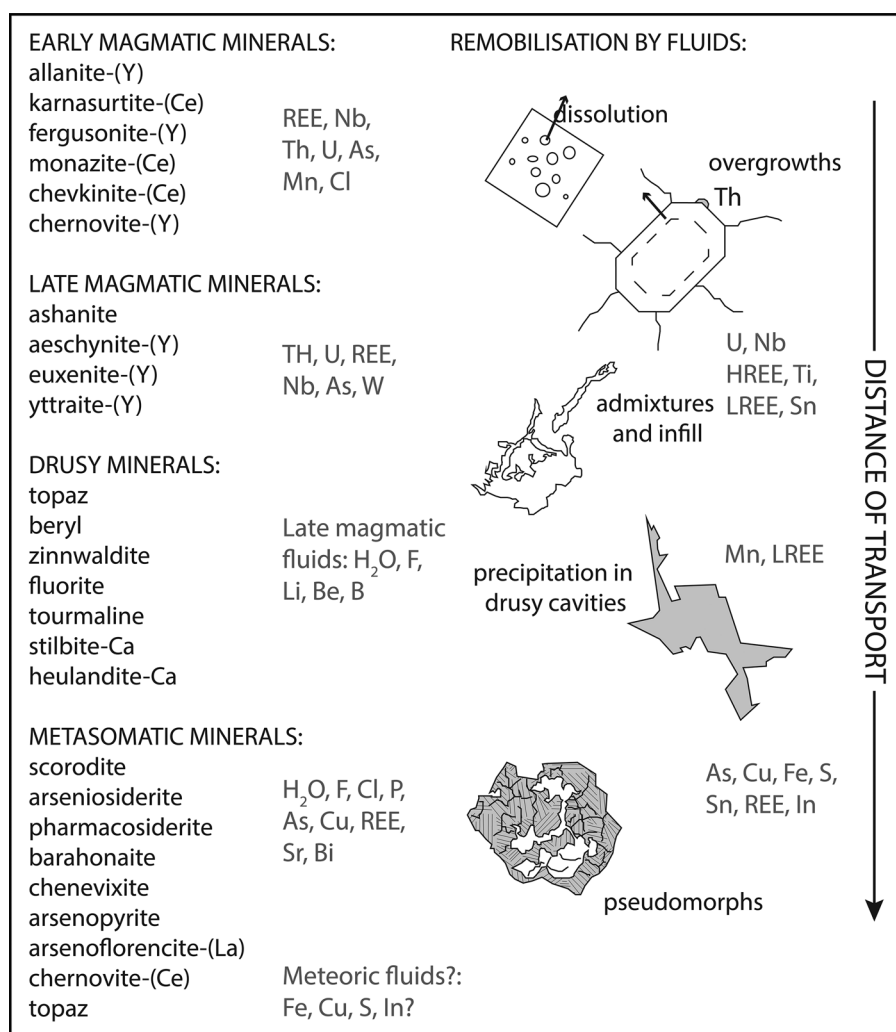


Fig. 15. Summary sketch diagram depicting minerals that crystallized during the petrogenesis of critical element enrichments, and their geochemical profile. Note that the figure is organized by petrogenetic process, rather than by anomaly type, and the distances of geochemical transport of geochemical tracers are sketched. The granitoid-forming minerals are omitted and the drusy mineral assemblage largely derives from the literature (Green *et al.* 2005).

fluids were heterogeneously distributed in small pockets in the roof zones of granitic magma chambers. Exsolution of multiple fluids in such magmatic environments have previously been shown to have significant compositional heterogeneity (Kamenetsky *et al.* 2002). Drusy topaz $\text{Al}_2\text{SiO}_4(\text{F},\text{OH})_2$, beryl ($\text{Be}_3\text{Al}_2\text{Si}_6\text{O}_{18}$), zinnwaldite (a lithium-iron mica), fluorite (CaF_2) and tourmaline (B-bearing aluminosilicate) are heterogeneously distributed amongst the drusy cavities but overall describe the composition of late-stage magmas that are very hydrous and rich in F, Be, Li and B.

The solubility of beryl falls with decreasing temperature and a low Be-content is required to saturate any granitic melt at the low temperatures of pegmatite formation (Evensen *et al.* 1999), such that the presence of beryl in the drusy cavities within magmas undergoing eutectic crystallization is not surprising. However, studies of beryl-hosted fluid inclusions have indicated that melt-fluid immiscibility can occur during crystallization (Thomas *et al.* 2009). The solubility of beryl is increased in the presence of Li, F and B (Evensen *et al.* 1999), and rare metal pegmatites of the Li-Cs-Ta family contain elevated Ta, Nb, Sn, Li, F and B amongst other elements (Thomas *et al.* 2009; Linnen *et al.* 2012). Where lithium resides in zinnwaldite that crystallized from fluids, which exsolved from late-fractionated granitic melt or as a greisenization product, it increased fluid pH and lead to destabilization of fluoride complexes, precipitation of metal oxides or inclusion of Sn in micas (Breiter *et al.* 2019; Ghosh *et al.* 2023). The occurrence of drusy biotite and zinnwaldite in roof zone rocks in the G1 granites and muscovitization of biotite in G2 granites (Fig. 9) suggest that micas may have influenced the conditions under which the late-stage fluids precipitated cassiterite (anomaly type 1) and the metasomatic

assemblage of topaz and arsenic-oxide-hydroxide minerals (anomaly type 2) in the Mourne Mountains.

In the G2 drusy granites, preferential partitioning of Nb + REE into eutectic magmatic minerals, and of Li, F, Be and B ± Sn into pockets of late-stage magmas/magmatic fluids is consistent with HFSE and REE-enrichment by differentiation through fractional crystallization and heterogeneous distribution of F-rich silicic residual melts (Boily and Williams-Jones 1994). At Pitinga, Brazil, enrichment in Sn, Nb, Ta, F (Y, REE, Li) occurs in peralkaline to metaluminous granites with high F-activity at hypersolvus temperatures and formation of Sn deposits is attributed to an abrupt magmatic-hydrothermal transition (Bastos Neto *et al.* 2009; Costi *et al.* 2009). Chloride species transport the REE in most hydrothermal systems, until there is an increase in pH or a decrease in Cl-activity, and then F and P act as binding agents for REE, promoting the formation of bastnäsite and monazite-(Ce) that have low solubility (Williams-Jones *et al.* 2012). These fluorocarbonate minerals occur in mineral pseudomorphs in metasomatic associations that overprint G2 granite (e.g. EM2, Pollaphuca), where topaz is an abundant metasomatic phase. The mineralogical comparisons strongly support the hypothesis that metasomatic fluids are derived dominantly from a magmatic source.

It is generally the case that REE occurrences that are economically viable cannot be explained by magmatic processes alone, and late-stage hydrothermal-metasomatic fluids are important to remobilize and concentrate REE (Chakhmouradian and Wall 2012; Williams-Jones *et al.* 2012; Smith *et al.* 2016). This is illustrated by some notable examples in Canada that have higher critical metal concentrations than the Mourne Mountains Granites:

The Strange Lake deposit (66 million tonnes at a grade of 1.52 wt% REE₂O₃) of Québec-Labrador and the Thor Lake deposit (1.73 million tonnes in the T-zone rare metal deposit, with grades of 0.1–0.17 wt% Y₂O₃, 0.2–0.28 REE₂O₃, 0.46–0.58 wt% Nb₂O₅) in the NW Territories (Taylor and Pollard 1996; Williams-Jones *et al.* 2012). REE in primary magmatic pyrochlore, zircon and monazite-(Ce) in the Strange Lake deposit were remobilized over a temperature range of 350°C to <150°C by sodic magmatic brines that interacted with calcic brines (Salvi and Williams-Jones 1996). The resulting hydrothermal assemblage included allanite-(Ce), gadolinite-(Y) and kainosite-(Y) and was largely confined to the pegmatites (Williams-Jones *et al.* 2012).

Whereas the Strange Lake deposit is characterized by HREE-bearing minerals local to the source minerals in pegmatites, metasomatic-hydrothermal mineralization at Thor Lake contains LREE-bearing fluorocarbonates and cross-cuts a gradational contact between syenites and granites (Taylor and Pollard 1996). Thor Lake fluorocarbonates, such as bastnasite-(Ce) and parasite-(Ce), form common mineral pseudomorphs, which are overprinted by later hydrothermal assemblages. Fluid inclusion and stable isotope investigations indicate that saline hydrothermal fluids had a single magmatic source and boiled at approximately 350°C (Taylor and Pollard 1996), which is in contrast with the evidence from zinnwaldite in other granite-hosted mineralization (Thomas *et al.* 2009; Breiter *et al.* 2019; Ghosh *et al.* 2023).

The LREE have been experimentally shown to be more mobile than the HREE in hydrothermal fluids, such that there is fractionation along fluid flow paths with HREE restricted to the high-temperature input zone and LREE migrating away from it (Williams-Jones *et al.* 2012). This pattern is also observed in the Mourne Mountains granites: primary xenotime-(Y)- and aeschnite-(Y)-bearing inclusions are leached from zircons and Fe–Ti oxide minerals (producing spongy dissolution textures) and are locally reprecipitated as secondary euxenite-(Y) and aeschnite-(Y) while REE minerals in metasomatic rocks are dominated by LREE-enriched monazite-(Ce) and bastnäsite-(Ce), and subsequently arsenoflorentite-(La) and chernovite-(Y).

The low quantities and fine grain-size of bastnäsite-(Ce), monazite-(Ce) and xenotime-(Y) throughout the Mourne granites (Fig. 13), are not as amenable to processing as those in the economic deposits. Xenotime-(Y) is an ideal source mineral for HREE but it is rare and restricted to an inclusion assemblage in G2 granite. Larger primary allanite-(Ce) and zircon crystals in the Mourne granites, particularly G1 granite, are silicate minerals that are resistant to chemical processing (Mariano and Mariano 2012). HREE-bearing oxides such as fergusonite-(Y), brannerite and euxenite-(Y) have attractive REE contents but are of small outcrop and require advances in REE recovery to pave the way for the development of granite-based polymetallic projects (Chakhmouradian and Zaitsev 2012). The discrete, small-scale nature of the mineralogical anomalies located using the stream and soil data is a reflection of the close-spaced sampling of the Tellus survey. These characteristics, coupled with conflicting outcomes from chemical and mineralogical indicators (a Nb/Ta based chemical classification as ‘barren’ and Hf-rich zircons: Alekseev and Alekseev 2020; Ballouard *et al.* 2020) do not indicate that the Mourne Mountains are prospective for REE. However, the Mourne Mountains and other granites of the BIPIP are reported as prospective in a recent report by the British Geological Survey (Deady *et al.* 2023).

The Mourne Mountains Granite Complex is not an isolated, nor a strongly peralkaline, granite complex in the British Tertiary Province and there are marked similarities between the Mourne Granites and the Arran Northern granite. The miarolitic/drusy cavities in the Arran granite contain fergusonite-(Y), gadolinite, allanite-(Ce) and zircon as accessory minerals accompanying topaz and beryl, and the granite groundmass includes allanite-(Ce),

zircon, apatite and fluorite (England 1992; Hyslop *et al.* 1999). The presence of the F- and P-rich minerals illustrates that a similar enrichment in Nb, La, Ce, Sm, Tb, and Y is a function of extensive fractional crystallization (England 1992) to a F-rich and volatile-dominated residual magma. This research may also provide some understanding of granites of Caledonian age (Gallagher *et al.* 1992; Ghani and Atherton 2006) in Ireland that are prospective for REE. F-rich melts and/or late-stage hydrothermal fluids have been suggested as the agents that concentrated HREE in the most evolved pegmatitic leucogranites of the late Caledonian Galway Batholith (Feely *et al.* 1991; Whitworth and Feely 2011), where late crystallized xenotime-(Y), monazite-(Ce), thorite and uraninite are spatially associated with fluorite, topaz and tourmaline. The Donegal granite, also late Caledonian, is known to host U-mineralization that is associated with both biotite-pegmatites and tectonic lineaments (O’Connor and Long 1985), which may be accompanied by REE-hosting minerals.

Conclusions

The largest anomalies in the survey data with greatest enrichment of critical and other technology metals in the Mourne Mountains are associated with: 1, late-stage and low temperature (eutectic) magmatic crystallization in the roof zones of the most peralkaline and mafic of the granitoid intrusions (G1 and G2) and, 2, evolved magmatic fluids that have either migrated locally or been focused by geological structures across the solidified roof zones of granitoid intrusions (G2). It appears that in the G2 drusy granites there is a preferential partitioning of Nb + REE into magmatic minerals while Li, Be, B, As, Sn, Mn³⁺ and Ce⁴⁺ partition into pockets of late-stage heterogeneously distributed F-rich silicic residual melts and relatively oxidizing halide-rich magmatic fluids. The fluids remobilize Nb + REE. Reactions between larger fluxes of magmatic fluids concentrated along structural features and mafic silicate + diverse accessory minerals in G2 drusy granites produced an As-rich metasomatic assemblage that hosts multiple base and critical metals. The critical metal anomalies in the Tellus deep soil data for the eastern Mourne agree well with the mineralogical associations and mineral chemistry observed in bedrock samples. The majority of mineralization is explained by crystallization at the eutectic and the magmatic hydrothermal transition, and exsolution of magmatic fluids. The role of muscovitization in changing fluid pH and F stability is likely very important in generating metasomatism and the development of granite-hosted greisen mineralization. The role of externally-derived hydrothermal or meteoric fluids was small. Mineral hosts to critical metal enrichments in the western Mourne did not satisfactorily explain additional diverse, small-scale anomalous features in the Tellus deep soil data, which we are investigating using heavy mineral concentrates. It does not appear likely that the mineralization will satisfy any of the constraints that would serve to make the mineral occurrences economic, but the region remains prospective and the regional survey data works well to direct research attention towards sample locations that can generate data to inform the creation of geomodels.

Acknowledgements The research was supported by the ‘Tellus Border’ INTERREG IVA programme of the European Regional Development Fund, managed by the Geological Survey of Northern Ireland (GSNI) and the Geological Survey of Ireland (GSI). The Tellus project was financed by the Department of Enterprise, Trade and Investment (DETI) and the Rural Development Programme in Northern Ireland. This research was completed under DETI/GSNI Scientific Services for the Tellus Border Project, reference 10761. The authors gratefully acknowledge the analytical and mineralogical expertise of Lorraine Field at the British Geological Survey. Alex Donald and Marie Cowan of GSNI and Kate Knights of GSI are acknowledged for assistance with provision of Tellus data, project management and internal reviews. We acknowledge very helpful feedback and review from A. Tindle, K. Goodenough, B. Simons, and an anonymous reviewer.

Author contributions KRM: conceptualization (lead), data curation (lead), formal analysis (lead), funding acquisition (lead), investigation (lead), methodology (lead), project administration (lead), validation (equal), visualization (lead), writing – original draft (lead), writing – review & editing (lead); NRM: conceptualization (supporting), data curation (supporting), formal analysis (supporting), investigation (supporting), validation (equal), writing – review & editing (supporting); GKR: data curation (supporting), formal analysis (supporting), investigation (supporting), validation (equal), writing – review & editing (supporting); PAJL: conceptualization (supporting), data curation (supporting), formal analysis (supporting), methodology (supporting), visualization (supporting), writing – review & editing (supporting)

Funding The Geological Survey of Northern Ireland (GSNI) and Department of Enterprise, Trade and Investment (DETI) awarded a contract for Scientific Services for the Tellus Border Project 10761, with Tellus supported by Interreg IVA.

Competing interests The authors declare that they have no known competing financial interests or personal relationships that could have appeared to influence the work reported in this paper. The lead author wishes to declare that they are a member of the Geoenergy Editorial Board, and had no influence over the handling of the manuscript.

Data availability The Tellus survey data is Open Access and can be accessed at <https://www.gsi.ie/en-ie/programmes-and-projects/tellus/Pages/default.aspx>. The majority of the remaining data is summarized in the tables presented in this article.

References

- Adam, J. and Green, T. 2006. Trace element partitioning between mica- and amphibole-bearing garnet ilmenite and hydrous basaltic melt: 1. Experimental results and the investigation of controls on partitioning behaviour. *Contributions to Mineralogy and Petrology*, **152**, 1–17, <https://doi.org/10.1007/s00410-006-0085-4>
- Alekseev, V.I. and Alekseev, I.V. 2020. Zircon as a mineral indicating the stage of granitoid magmatism at Northern Chukotka, Russia. *Geosciences (Switzerland)*, **10**, <https://doi.org/10.3390/geosciences10050194>
- Andersen, J.C.Ø., Rollinson, G.K., Snook, B., Herrington, R. and Fairhurst, R.J. 2009. Use of QEMSCAN® for the characterization of Ni-rich and Ni-poor goethite in laterite ores. *Minerals Engineering*, **22**, 1119–1129, <https://doi.org/10.1016/j.mineng.2009.03.012>
- Arthurs, J.W. and Earls, G. 2004. Minerals. In: Mitchell, W.I. (ed.) *The Geology of Northern Ireland – Our Natural Foundation*, Geological Survey of Northern Ireland, 255–272.
- ASTM-Standard-E1508 2012. Designation: E1508-12a. *Standard Guide for Quantitative Analysis by Energy-Dispersive Spectroscopy*, <https://doi.org/10.1520/E1508-12A>
- Balouard, C., Pujol, M., Boulvais, P., Branquet, Y., Tartèse, R. and Vigneresse, J.L. 2016. Nb-Ta fractionation in peraluminous granites: a marker of the magmatic-hydrothermal transition. *Geology*, **44**, 231–234, <https://doi.org/10.1130/G37475.1>
- Balouard, C., Elburg, M.A., Tappe, S., Reinke, C., Ueckermann, H. and Daggart, S. 2020. Magmatic-hydrothermal evolution of rare metal pegmatites from the Mesoproterozoic Orange River pegmatite belt (Namaqualand, South Africa). *Ore Geology Reviews*, **116**, 103252, <https://doi.org/10.1016/j.oregeorev.2019.103252>
- Banks, G.J., Walter, B.F., Marks, M.A.W. and Siegfried, P.R. 2019. A workflow to define, map and name a carbonate- or alkaline igneous-associated REE-HFSE mineral system: a case study from SW Germany. *Minerals*, **9**, <https://doi.org/10.3390/min9020097>
- Banks, G.J., Olsen, S.D. and Gusak, A. 2020. A method to evaluate REE-HFSE mineralised provinces by value creation potential, and an example of application: Gardar REE-HFSE province, Greenland. *Geoscience Frontiers*, **11**, 2141–2156, <https://doi.org/10.1016/j.gsf.2020.05.019>
- Bastos Neto, A.C., Pereira, V.P., Ronchi, L.H., De Lima, E.F. and Frantz, J.C. 2009. The world-class Sn, Nb, Ta, F (Y, REE, Li) Deposit and the massive cryolite associated with the albite-enriched facies of the madeira a-type granite, Pitinga Mining District, Amazonas State, Brazil. *Canadian Mineralogist*, **47**, 1329–1357, <https://doi.org/10.3749/canmin.47.6.1329>
- Bazley, R.A.B. 2004. Chapter 18: Quaternary. In: Mitchell, W.I. (ed.) *The Geology of Northern Ireland – Our Natural Foundation*, Geological Survey of Northern Ireland, 211–226.
- Bertrand, G., Cassard, D., Arvanitidis, N. and Stanley, G. 2016. Map of critical raw material deposits in Europe. *Energy Procedia*, **97**, 44–50, <https://doi.org/10.1016/j.egypro.2016.10.016>
- BGS 2022. *UK Criticality Assessment of Technology Critical Minerals and Metals*. Decarbonisation & Resource Management Commissioned Report **CR/21/120**.
- Binnemans, K., Jones, P.T., Blanpain, B., Van Gerven, T., Yang, Y., Walton, A. and Buchert, M. 2013. Recycling of rare earths: a critical review. *Journal of Cleaner Production*, **51**, 1–22, <https://doi.org/10.1016/j.jclepro.2012.12.037>
- Bloodworth, A. 2014. Track flows to manage technology-metal supply. *Nature*, **505**, 9–10, <https://doi.org/10.1038/505019a>
- Boily, M. and Williams-Jones, A.E. 1994. The role of magmatic and hydrothermal processes in the chemical evolution of the Strange Lake plutonic complex, Quebec-Labrador. *Contributions to Mineralogy and Petrology*, **118**, 33–47, <https://doi.org/10.1007/BF00310609>
- Breiter, K., Hložková, M., Korbelová, Z. and Galiová, M.V. 2019. Diversity of lithium mica compositions in mineralized granite–greisen system: Cínovec Li-Sn-W deposit, Erzgebirge. *Ore Geology Reviews*, **106**, 12–27, <https://doi.org/10.1016/j.oregeorev.2019.01.013>
- Chakhmouradian, A.R. and Wall, F. 2012. Rare earth elements: minerals, mines, magnets (and more). *Elements*, **8**, 333–340, <https://doi.org/10.2113/gselements.8.5.333>
- Chakhmouradian, A. and Zaitsev, A. 2012. Rare earth mineralisation in igneous rocks: sources and processes. *Elements*, **8** SRC-G, 347–353, <https://doi.org/10.2113/gselements.8.5.347>
- Chakhmouradian, A.R., Smith, M.P. and Kynicky, J. 2015. From ‘strategic’ tungsten to ‘green’ neodymium: a century of critical metals at a glance. *Ore Geology Reviews*, **64**, 455–458, <https://doi.org/10.1016/j.oregeorev.2014.06.008>
- Chevychev, V.Y., Zaraisky, G.P., Borisovskii, S.E. and Borkov, D.A. 2005. Effect of melt composition and temperature on the partitioning of Ta, Nb, Mn, and F between granitic (alkaline) melt and fluorine-bearing aqueous fluid: fractionation of Ta and Nb and conditions of ore formation in rare-metal granites. *Petrology*, **13**, 305–321.
- Conliffe, J. and Feely, M. 2010. Fluid inclusions in Irish granite quartz: monitors of fluids trapped in the onshore Irish Massif. *Earth and Environmental Science Transactions of the Royal Society of Edinburgh*, **101**, 53–66, <https://doi.org/10.1017/s1755691010009047>
- Cooper, M.R., Anderson, H., Walsh, J.J., Van Dam, C.L., Young, M.E., Earls, G. and Walker, A. 2012. Palaeogene Alpine tectonics and Icelandic plume-related magmatism and deformation in Northern Ireland. *Journal of the Geological Society*, **169**, 29–36, <https://doi.org/10.1144/0016-76492010-182>
- Costanzo, A., Moore, K.R., Wall, F. and Feely, M. 2006. Fluid inclusions in apatite from Jacupiranga calcite carbonatites: evidence for a fluid-stratified carbonate magma chamber. *Lithos*, **91**, 208–228, <https://doi.org/10.1016/j.lithos.2006.03.047>
- Costi, H.T., Dall’Agnol, R., Pichavant, M. and Rämö, O.T. 2009. The peralkaline tin-mineralized madeira cryolite albite-rich granite of pitinga, amazonian craton, brazil: Petrography, mineralogy and crystallization processes. *Canadian Mineralogist*, **47**, 1301–1327, <https://doi.org/10.3749/canmin.47.6.1301>
- Deady, E., Goodenough, K.M. et al. 2023. *Potential for Critical Raw Material Prospectivity in the UK*. Decarbonisation and Resource Management Programme, Commissioned Report **CR/23/024**.
- Du, X. and Graedel, T.E. 2011. Uncovering the global life cycles of the rare earth elements. *Scientific Reports*, **1**, 145, <https://doi.org/10.1038/srep00145>
- Earls, G. 2016. Mineral resources and Tellus: the essential balance. In: Young, M.E. (ed.) *Unearthed: Impacts of the Tellus Surveys of the North of Ireland*, Royal Irish Academy, Dublin, 67–74, <https://doi.org/10.2307/j.ctt1g69w6r.10>
- Emeleus, C.H. 1955. The granites of the western Mourne Mountains, County Down. *Scientific Proceedings of the Royal Dublin Society*, **27**, 35–50.
- England, R.W. 1992. The genesis, ascent, and emplacement of the Northern Arran Granite, Scotland: implications for granitic diapirism. *Geological Society of America Bulletin*, **104**, 606–614, [https://doi.org/10.1130/0016-7606\(1992\)104<0606:TGAEO>2.3.CO;2](https://doi.org/10.1130/0016-7606(1992)104<0606:TGAEO>2.3.CO;2)
- Ercit, T.S. 2005. Identification and alteration trends of granitic-pegmatite-hosted (Y,REE,U,Th)-(Nb,Ta,Ti) oxide minerals: a statistical approach. *Canadian Mineralogist*, **43**, 1291–1303, <https://doi.org/10.2113/gscanmin.43.4.1291>
- Ermolaeva, V.N., Pekov, I.V., Chukanov, N.V. and Zadov, A.E. 2007. Thorium mineralization in hyperalkaline pegmatites and hydrothermalites of the Lovozero pluton, Kola Peninsula. *Geology of Ore Deposits*, **49**, 758–775, <https://doi.org/10.1134/S1075701507080107>
- European Commission 2023. *Study on the Critical Raw Materials for the EU*. Final Report, <https://doi.org/10.2873/725585>
- Evensen, J.M., London, D. and Wendlandt, R.F. 1999. Solubility and stability of beryl in granitic melts. *American Mineralogist*, **84**, 733–745, <https://doi.org/10.2138/am-1999-5-605>
- Ewing, R.C. 1976. A numerical approach toward the classification of complex, orthorhombic, rare-earth, AB₂O₆-type Nb-Ta-Ti oxides. *The Canadian Mineralogist*, **14**, 111–119.
- Feely, M., McCabe, E. and Kundendorf, H. 1991. The evolution of REE profiles in the Galway Granite Western Ireland. *Irish Journal of Earth Sciences*, **11**, 71–89.
- Gallagher, V., Feely, M., Högelsberger, H., Jenkin, G.R.T. and Fallick, A.E. 1992. Geological, fluid inclusion and stable isotope studies of Mo mineralization, Galway Granite, Ireland. *Mineralium Deposita*, **27**, 314–325, <https://doi.org/10.1007/BF00193402>
- Gamble, J.A., Wysockanski, R.J. and Meighan, I.G. 1999. Constraints on the age of the British Tertiary Volcanic Province from ion microprobe U-Pb (SHRIMP) ages for acid igneous rocks from NE Ireland. *Journal of the Geological Society*, **156**, 291–299, <https://doi.org/10.1144/gsjgs.156.2.0291>

- Ganerød, M., Chew, D.M., Smethurst, M.A., Troll, V.R., Corfú, F., Meade, F. and Prestvik, T. 2011. Geochronology of the Tardree Rhyolite Complex, Northern Ireland: implications for zircon fission track studies, the North Atlantic Igneous Province and the age of the Fish Canyon sanidine standard. *Chemical Geology*, **286**, 222–228, <https://doi.org/10.1016/j.chemgeo.2011.05.007>
- Ghani, A.A. and Atherton, M.P. 2006. The chemical character of the Late Caledonian Donegal Granites, Ireland, with comments on their genesis. *Transactions of the Royal Society of Edinburgh, Earth Sciences*, **97**, 437–454, <https://doi.org/10.1017/S0263593300001553>
- Ghosh, U., Upadhyay, D., Mishra, B. and Abhinay, K. 2023. In-situ trace element and Li-isotope study of zinnwaldite from the Degana tungsten deposit, India: implications for hydrothermal tungsten mineralization. *Chemical Geology*, **632**, 121550, <https://doi.org/10.1016/j.chemgeo.2023.121550>
- Gibson, D. 1984. *The Petrology and Geochemistry of the Western Mourne Granites, Co. Down, N. Ireland*. PhD thesis, The Queen's University of Belfast.
- Gibson, D., McCormick, A.G., Meighan, I.G. and Halliday, A.N. 1987. The British Tertiary Igneous Province: young Rb-Sr ages for the Mourne Mountains Granites. *Scottish Journal of Geology*, **23**, 221–225, <https://doi.org/10.1144/sjg23020221>
- Gibson, D., Meighan, I.G. and Gamble, J.A. 2003. Magmatic pulses in the Western Mourne Tertiary Center, NE Ireland. In: Geological Society of America Northeastern Section 38th Annual Meeting.
- Gillis, K.M. and Roberts, M.D. 1999. Cracking at the magma-hydrothermal transition: evidence from the Troodos Ophiolite, Cyprus. *Earth and Planetary Science Letters*, **169**, 227–244, [https://doi.org/10.1016/S0012-821X\(99\)00087-4](https://doi.org/10.1016/S0012-821X(99)00087-4)
- Glasby, G.P., Gwozdz, R., Kunzendorf, H., Friedrich, G. and Thijssen, T. 1987. The distribution of rare earth and minor elements in manganese nodules and sediments from the equatorial and S.W. Pacific. *Lithos*, **20**, 97–113, [https://doi.org/10.1016/0024-4937\(87\)90001-6](https://doi.org/10.1016/0024-4937(87)90001-6)
- Godfrey, L.V., Lee, D.-C., Sangrey, W.F., Halliday, A.N., Hein, J.R., White, W.M. and Salters, V.J.M. 1997. The Hf isotopic composition of ferromanganese nodules and crusts and hydrothermal manganese deposit: implications for seawater Hf. *Earth and Planetary Science Letters*, **151**, 91–105, [https://doi.org/10.1016/S0012-821X\(97\)00106-4](https://doi.org/10.1016/S0012-821X(97)00106-4)
- Goodenough, K.M., Schilling, J. *et al.* 2016. Europe's rare earth element resource potential: an overview of REE metallogenetic provinces and their geodynamic setting. *Ore Geology Reviews*, **72**, 838–856, <https://doi.org/10.1016/j.oregeorev.2015.09.019>
- Graedel, T.E., Barr, R. *et al.* 2012. Methodology of metal criticality determination. *Environmental Science and Technology*, **46**, 1063–1070, <https://doi.org/10.1021/es203534z>
- Graedel, T.E., Gunn, G. and Espinoza, L.T. 2014. 1 Metal resources, use and criticality. In: Gunn, G. (ed.) *Critical Metals Handbook*, John Wiley & Sons, 1–19, <https://doi.org/10.1002/9781118755341.ch1>
- Graedel, T.E., Harper, E.M., Nassar, N.T., Nuss, P. and Reck, B.K. 2015. Criticality of metals and metalloids. *Proceedings of the National Academy of Sciences*, **112**, 4257–4262, <https://doi.org/10.1073/pnas.1500415112>
- Green, T.H. 1995. Significance of Nb/Ta as an indicator of geochemical processes in the crust-mantle system. *Chemical Geology*, **120**, 347–359, [https://doi.org/10.1016/0009-2541\(94\)00145-X](https://doi.org/10.1016/0009-2541(94)00145-X)
- Green, D.I., Bell, R. and Moreton, S. 2005. Drusy cavity minerals including the first Irish danalite from Lindsay's Leap, Mourne Mountains. *UK Journal of Mines & Minerals*, **25**, 25–30.
- Haberlah, D., Strong, C., Pirrie, D., Rollinson, G.K., Gottlieb, P., Botha, P.W.S.K. and Butcher, A.R. 2011. Automated petrography applications in Quaternary Science. *Quaternary Australia*, **28**, 3–12, <http://hdl.handle.net/10072/45844>
- Hagelüken, C. and Goldmann, D. 2022. Recycling and circular economy – towards a closed loop for metals in emerging clean technologies. *Mineral Economics*, **35**, 539–562, <https://doi.org/10.1007/s13563-022-00319-1>
- Hansen, J., Jerram, D.A., McCaffrey, K. and Passey, S.R. 2009. The onset of the North Atlantic Igneous Province in a rifting perspective. *Geological Magazine*, **146**, 309, <https://doi.org/10.1017/S0016756809006347>
- Harding, R.R., Merriman, R.J. and Nancarrow, P.H.A. 1982. A Note on the Occurrence of chevkinite, allanite and kirkelite on St. Kilda, Scotland. *Mineralogical Magazine*, **46**, 445–448, <https://doi.org/10.1180/minmag.1982.046.341.06>
- Hayes, S.M. and McCullough, E.A. 2018. Critical minerals: a review of elemental trends in comprehensive criticality studies. *Resources Policy*, **59**, 192–199, <https://doi.org/10.1016/j.resourpol.2018.06.015>
- Hodgson, J. and Young, M. 2016. The Tellus airborne geophysical surveys and results. In: Young, M. (ed.) *Unearthed: Impacts of the Tellus Surveys of the North of Ireland*, Royal Irish Academy, Dublin, 11–31, <https://doi.org/10.2307/j.ctt1g69w6r.7>
- Hole, M.J. and Millett, J.M. 2016. Controls of mantle potential temperature and lithospheric thickness on magmatism in the North Atlantic Igneous Province. *Journal of Petrology*, **57**, 417–436, <https://doi.org/10.1093/petrology/egw014>
- Honour, V.C., Goodenough, K.M., Shaw, R.A., Gabudianu, I. and Hirtopanu, P. 2018. REE mineralisation within the Ditrău Alkaline Complex, Romania: interplay of magmatic and hydrothermal processes. *Lithos*, **314–315**, 360–381, <https://doi.org/10.1016/j.lithos.2018.05.029>
- Hood, D.N. 1981. *Geochemical, Petrological and Structural Studies on the Tertiary Granites and Associated Rocks of the Eastern Mourne Mountains, Co. Down, Northern Ireland*. PhD thesis, The Queen's University of Belfast.
- Hornig-Kjarsgaard, I. 2008. Rare-Earth Elements in Soviec Carbonatites and their Mineral Phases. *Journal of Petrology*, **39**, 2105–2121, <https://doi.org/10.1093/ptro/39.11-12.2105>
- Hu, X., Bi, X., Shang, L., Hu, R., Cai, G. and Chen, Y. 2009. An experimental study of tin partition between melt and aqueous fluid in F/Cl-coexisting magma. *Chinese Science Bulletin*, **54**, 1087–1097, <https://doi.org/10.1007/s11434-009-0008-7>
- Hughes, H.S.R., Boyce, A.J., McDonald, I., Davidheiser-Kroll, B., Holwell, D.A., McDonald, A. and Oldroyd, A. 2015. Contrasting mechanisms for crustal sulphur contamination of mafic magma: evidence from dyke and sill complexes from the British Palaeogene Igneous Province. *Journal of the Geological Society*, **172**, 443–458, <https://doi.org/10.1144/jgs2014-112>
- Hyslop, E.K., Gillanders, R.J., Hill, P.G. and Fakes, R.D. 1999. Rare-earth-bearing minerals fergusonite and gadolinite from the Arran granite. *Scottish Journal of Geology*, **35**, 65–69, <https://doi.org/10.1144/sjg35010065>
- Johnson, C., Breward, N., Ander, E.L. and Ault, L. 2005. G-BASE: baseline geochemical mapping of Great Britain and Northern Ireland. *Geochemistry: Exploration, Environment, Analysis*, **5**, 347–357, <https://doi.org/10.1144/1467-7873/05-070>
- Jolley, D.W. and Bell, B.R. 2002. The evolution of the North Atlantic Igneous Province and the opening of the NE Atlantic rift. *Geological Society, London, Special Publications*, **197**, 1–13, <https://doi.org/10.1144/GSL.SP.2002.197.01.01>
- Kaeter, D., Barros, R., Menuge, J.F. and Chew, D.M. 2018. The magmatic-hydrothermal transition in rare-element pegmatites from southeast Ireland: LA-ICP-MS chemical mapping of muscovite and columbite-tantalite. *Geochimica et Cosmochimica Acta*, **240**, 98–130, <https://doi.org/10.1016/j.gca.2018.08.024>
- Kamenetsky, V.S., van Acherbergh, E., Ryan, C.G., Naumov, V.B., Mernagh, T.P. and Davidson, P. 2002. Extreme chemical heterogeneity of granite-derived hydrothermal fluids: an example from inclusions in a single crystal of miarolitic quartz. *Geology*, **30**, 459–462, [https://doi.org/10.1130/0091-7613\(2002\)030<0459:ECHOGD>2.0.CO;2](https://doi.org/10.1130/0091-7613(2002)030<0459:ECHOGD>2.0.CO;2)
- Kent, R.Y.W. and Fitton, J.G. 2000. Mantle sources and melting dynamics in the British Palaeogene Igneous Province. *Journal of Petrology*, **41**, 1023–1040, <https://doi.org/10.1093/ptrology/41.7.1023>
- Kügerl, M.T., Hitch, M. and Gugerell, K. 2023. Responsible sourcing for energy transitions: discussing academic narratives of responsible sourcing through the lens of natural resources justice. *Journal of Environmental Management*, **326**, 116711, <https://doi.org/10.1016/j.jenvman.2022.116711>
- Linnen, R.L. and Keppler, H. 1997. Columbite solubility in granitic melts: consequences for the enrichment and fractionation of Nb and Ta in the Earth's crust. *Contributions to Mineralogy and Petrology*, **128**, 213–227, <https://doi.org/10.1007/s004100050304>
- Linnen, R.L., Van Lichtervelde, M. and Černý, P. 2012. Granitic pegmatites as sources of strategic metals. *Elements*, **8**, 275–280, <https://doi.org/10.2113/gselements.8.4.275>
- Liu, X.H., Li, B. *et al.* 2022. Monazite geochronology and geochemistry constraints on the formation of the giant Zhengchong Li-Rb-Cs deposit in South China. *Ore Geology Reviews*, **150**, 105147, <https://doi.org/10.1016/j.oregeorev.2022.105147>
- Lusty, P. 2016. Critical metals for high- technology applications: mineral exploration potential in the north of Ireland. In: Young, M. (ed.) *Unearthed: Impacts of the Tellus Surveys of the North of Ireland*, Royal Irish Academy, Dublin, 101–117, <https://doi.org/j.ctt1g69w6r.13> [COMP: publisher name inserted in Lusty 2016]
- Lusty, P.A.J. and Gunn, A.G. 2014. Challenges to global mineral resource security and options for future supply. *Geological Society, London, Special Publications*, **393**, 265–276, <https://doi.org/10.1144/SP393.13>
- MacDonald, R., Baginski, B., Dzierzanowski, P., Fettes, D.J. and Upton, B.G.J. 2013. Chevkinite-group minerals in UK Palaeogene granites: underestimated REE-bearing accessory phases. *Canadian Mineralogist*, **51**, 333–347, <https://doi.org/10.3749/canmin.51.2.333>
- Mariano, A.N. and Mariano, A., Jr 2012. Rare earth mining and exploration in North America. *Elements*, **8**, 369–376, <https://doi.org/10.2113/gselements.8.5.369>
- Mattsson, T., Burchardt, S., Mair, K. and Place, J. 2020. Host-rock deformation during the emplacement of the Mourne Mountains granite pluton: insights from the regional fracture pattern. *Geosphere*, **16**, 182–209, <https://doi.org/10.1130/GES02148.1>
- McAlister, J.J., Cooney, G. and Higgins, M.J. 1997. Accumulation of uranium in granitic soils overlying the Mourne Mountains, County Down, Northern Ireland. *Microchemical Journal*, **56**, 315–326, <https://doi.org/10.1006/mchj.1996.1399>
- McCabe, M. 2008. *Glacial Geology and Geomorphology: The Landscapes of Ireland*. Dunedin Academic Press.
- McCormick, A.G., Fallick, A.E., Harmon, R.S., Meighan, I.G. and Gibson, D. 1993. Oxygen and hydrogen isotope geochemistry of the Mourne Mountains Tertiary granites, Northern Ireland. *Journal of Petrology*, **34**, 1177–1202, <https://doi.org/10.1093/ptrology/34.6.1177>
- Meighan, I.G. and Gamble, J.A. 1972. Tertiary acid magmatism in NE Ireland. *Nature*, **240**, 183–184.

- Meighan, I.G., Gibson, D. and Hood, D.N. 1984. Some aspects of Tertiary acid magmatism in NE Ireland. *Mineralogical Magazine*, **48**, 351–363, <https://doi.org/10.1180/minmag.1984.048.348.05>
- Meighan, I.G., McCormick, A.G., Gibson, D., Gamble, J.A. and Graham, I.J. 1988. Rb-Sr isotopic determinations and the timing of Tertiary central complex magmatism in NE Ireland. *Geological Society, London, Special Publications*, **39**, 349–360, <https://doi.org/10.1144/GSL.SP.1988.039.01.30>
- Meighan, I., Fallick, A. and McCormick, A. 1992. Anorogenic granite magma genesis: new isotopic data for the southern sector of the British Tertiary Igneous Province. *Earth and Environmental Science Transactions of the Royal Society of Edinburgh*, **83**, 227–233, <https://doi.org/10.1017/S0263593300007914>
- Moffett, J.W. 1994. A radiotracer study of cerium and manganese uptake onto suspended particles in Chesapeake Bay. *Geochimica et Cosmochimica Acta*, **58**, 695–703, [https://doi.org/10.1016/0016-7037\(94\)90499-5](https://doi.org/10.1016/0016-7037(94)90499-5)
- Moles, N.R. and Higgins, M.J. 1995. Uranium distribution and radon potential in the Mournes, Northern Ireland. In: Pašava, J., Kříbek, B. and Žák, K. (eds) *Mineral Deposits: From Their Origin to Their Environmental Impacts*, Proceedings of the Third Biennial SGA Meeting, Prague, 685–688.
- Moles, N.R. and Tindle, A.G. 2011. Alluvial occurrences of fergusonite and gadolinite in the Mourne Mountains, Northern Ireland. *Journal of the Russell Society*, **14**, 1–3.
- Moles, N.R. and Tindle, A.G. 2012. Tungsten and bismuth minerals, including russellite, within greisen veins in the western Mourne Mountains, Northern Ireland. *Journal of the Russell Society*, **15**, 40–48.
- Moles, N.R., Chapman, R.J. and Warner, R.B. 2013. The significance of copper concentrations in natural gold alloy for reconnaissance exploration and understanding gold-depositing hydrothermal systems. *Geochemistry: Exploration, Environment, Analysis*, **13**, 115–130, <https://doi.org/10.1144/geochem2011-114>
- Moore, K., Moles, N. and Lusty, P. 2016. A natural laboratory for critical metals investigations in the Mourne Mountains granites. In: Young, M. (ed.) *Unearthed: Impacts of the Tellus Surveys of the North of Ireland*, Royal Irish Academy, Dublin, 119–128, <https://doi.org/10.2307/j.ctt1g69w6r.14> [COMP: Publisher inserted and doi updated]
- Moss, R.L., Tzimas, E., Kara, H., Willis, P. and Kooroshy, J. 2011. *Critical metals in strategic energy technologies - Assessing rare metals as supply-chain bottlenecks in low-carbon energy technologies*, Joint Research Centre, Institute for Energy and Transport. Publications Office, 2011 <https://data.europa.eu/doi/10.2790/35716>
- Nockolds, S.R. and Richey, J.E. 1939. Replacement veins in the Mourne Mountains Granites, N. Ireland. *American Journal of Science*, **237**, 27–47, <https://doi.org/10.2475/ajs.237.1.27>
- O'Connor, P.J. 1988. Strontium isotope geochemistry of Tertiary igneous rocks, NE Ireland. *Geological Society, London, Special Publications*, **39**, 361–363, <https://doi.org/10.1144/GSL.SP.1988.039.01.31>
- O'Connor, P.J. and Long, C.B. 1985. Radioelement abundance data for some Dalriadan rocks from Co. Donegal, Ireland. *Mineralogical Magazine*, **49**, 643–648, <https://doi.org/10.1180/minmag.1985.049.354.02>
- Pouchou, J.L., Pichoir, F. and Boivin, D. 1990. The XPP procedure applied to quantitative EDS X-ray analysis in the SEM. In: Michael, J.R. and Ingram, P. (eds) *Microbeam Analysis*. San Francisco Press, 120–126.
- Pourret, O., Davranche, M., Graau, G. and Dia, A. 2008. New insights into cerium anomalies in organic-rich alkaline waters. *Chemical Geology*, **251**, 120–127, <https://doi.org/10.1016/j.chemgeo.2008.03.002>
- Reck, B.K. and Graedel, T.E. 2012. Challenges in metal recycling. *Science*, **337**, 690–695, <https://doi.org/10.1126/science.1217501>
- Richey, J.E. 1928. The structural relations of the Mourne granites (Northern Ireland). *Quarterly Journal of the Geological Society*, **83**, 653–688, <https://doi.org/10.1144/GSL.JGS.1927.083.01-05.27>
- Rollinson, G.K., Andersen, J.C.Ø., Stickland, R.J., Boni, M. and Fairhurst, R. 2011. Characterisation of non-sulphide zinc deposits using QEMSCAN. *Minerals Engineering*, **24**, 778–787, <https://doi.org/10.1016/j.mineng.2011.02.004>
- Salvi, S. and Williams-Jones, A.E. 1996. The role of hydrothermal processes in concentrating high-field strength elements in the Strange Lake peralkaline complex, northeastern Canada. *Geochimica et Cosmochimica Acta*, **60**, 1917–1932, [https://doi.org/10.1016/0016-7037\(96\)00071-3](https://doi.org/10.1016/0016-7037(96)00071-3)
- Santoro, L., Boni, M., Rollinson, G.K., Mondillo, N., Balassone, P. and Clegg, A.M. 2014. Mineralogical characterization of the Hakkari nonsulfide Zn(Pb) deposit (Turkey): the benefits of QEMSCAN?? *Minerals Engineering*, **69**, 29–39, <https://doi.org/10.1016/j.mineng.2014.07.002>
- Schmidt, C., Romer, R.L., Wohlgeuth-Ueberwasser, C.C. and Appelt, O. 2020. Partitioning of Sn and W between granitic melt and aqueous fluid. *Ore Geology Reviews*, **117**, 103263, <https://doi.org/10.1016/j.oregeorev.2019.103263>
- Seymour, H.J. 1903. On the occurrence of cassiterite in Tertiary Granite of the Mourne Mountains. *Scientific Proceedings of the Royal Dublin Society*, **9**, 583–584.
- Shaw, R.A., Goodenough, K.M., Deady, E., Nex, P., Ruzvidzo, B., Rushton, J.C. and Mountney, I. 2022. The magmatic–hydrothermal transition in lithium pegmatites: petrographic and geochemical characteristics of pegmatites from the Kamativi Area, Zimbabwe. *Canadian Mineralogist*, **60**, 957–987, <https://doi.org/10.3749/canmin.2100032>
- Škoda, R. and Novák, M. 2007. Y,REE,Nb,Ta,Ti-oxide (AB₂O₆) minerals from REL-REE euxenite-subtype pegmatites of the Trebič Pluton, Czech Republic; substitutions and fractionation trends. *Lithos*, **95**, 43–57, <https://doi.org/10.1016/j.lithos.2006.07.020>
- Smith, M.P., Moore, K., Kavcicsánszki, D., Finch, A.A., Kynicky, J. and Wall, F. 2016. From mantle to critical zone: a review of large and giant sized deposits of the rare earth elements. *Geoscience Frontiers*, **7**, 315–334, <https://doi.org/10.1016/j.gsf.2015.12.006>
- Smyth, D. 2007. *Methods Used in the Tellus Geochemical Mapping of Northern Ireland*. British Geological Survey Open Report, **OR/07/022**.
- Steinbach, V. and Wellmer, F.W. 2010. Consumption and use of non-renewable mineral and energy raw materials from an economic geology point of view. *Sustainability*, **2**, 1408–1430, <https://doi.org/10.3390/su2051408>
- Steiner, B.M. 2018. Using Tellus stream sediment geochemistry to fingerprint regional geology and mineralisation systems in Southeast Ireland. *Irish Journal of Earth Sciences*, **36**, 45–61, <https://doi.org/10.1353/ijes.2018.0004>
- Steiner, B.M. 2019. Tools and workflows for grassroots Li-Cs-Ta (LCT) pegmatite exploration. *Minerals*, **9**, 24–26, <https://doi.org/10.3390/min9080499>
- Stepanov, A.S., Meffre, S., Mavrogenes, J. and Steadman, J. 2016. Nb-Ta fractionation in peraluminous granites: a marker of the magmatic-hydrothermal transition. *Geology*, **44**, e394, <https://doi.org/10.1130/G38086C.1>
- Stephenson, M.H., Ludden, J. et al. 2023. The need for joined-up thinking in critical raw materials research. *Geoenergy*, **1**, geoenergy2023-001, <https://doi.org/10.1144/geoenergy2023-001> [COMP: update Stephenson et al to journal reference. Doi updated]
- Stevenson, C.T.E. and Bennett, N. 2011. The emplacement of the Palaeogene Mourne Granite Centres, Northern Ireland: new results from the Western Mourne Centre. *Journal of the Geological Society*, **168**, 831–836, <https://doi.org/10.1144/0016-76492010-123>
- Stevenson, C.T.E., Owens, W.H., Hutton, D.H.W., Hood, D.N. and Meighan, I.G. 2007. Laccolithic, as opposed to cauldron subsidence, emplacement of the Eastern Mourne pluton, N. Ireland: evidence from anisotropy of magnetic susceptibility. *Journal of the Geological Society*, **164**, 99–110, <https://doi.org/10.1144/0016076492006-008>
- Storey, M., Duncan, R.A. and Tegner, C. 2007. Timing and duration of volcanism in the North Atlantic Igneous Province: implications for geodynamics and links to the Iceland hotspot. *Chemical Geology*, **241**, 264–281, <https://doi.org/10.1016/j.chemgeo.2007.01.016>
- Stuart, F.M., Ellam, R.M., Harrop, P.J., Fitton, J.G. and Bell, B.R. 2000. Constraints on mantle plumes from the helium isotopic composition of basalts from the British Tertiary Igneous Province. *Earth and Planetary Science Letters*, **177**, 273–285, [https://doi.org/10.1016/S0012-821X\(00\)00050-9](https://doi.org/10.1016/S0012-821X(00)00050-9)
- Sun, S.-S. and McDonough, W.F. 1989. Chemical and isotopic systematics of oceanic basalts: implications for mantle composition and processes. In: Saunders, A.D. and Norry, M.J. (eds) *Magmatism in the Ocean Basins*. Geological Society, London, Special Publications, **42**, 313–345, <https://doi.org/10.1144/GSL.SP.1989.042.01.19>
- Tammemagi, H.Y. 1976. Radioelement concentrations in British Tertiary Granites. *Geological Magazine*, **113**, 271–276, <https://doi.org/10.1017/S0016756800043259>
- Taylor, R.P. and Pollard, P.J. 1996. Rare earth element mineralization in peralkaline systems: the T-Zone REE-Y-Be deposit, Thor Lake, Northwest Territories, Canada. In: Jones, A.P., Wall, F. and Williams, C.T. (eds) *Rare Earth Minerals: Chemistry, Origin and Ore Deposits*, Springer, 167–192.
- Thomas, R., Davidson, P. and Badanina, E. 2009. A melt and fluid inclusion assemblage in beryl from pegmatite in the Orlovka amazonite granite, East Transbaikalia, Russia: implications for pegmatite-forming melt systems. *Mineralogy and Petrology*, **96**, 129–140, <https://doi.org/10.1007/s00710-009-0053-6>
- Thompson, P., Mussett, A.E. and Dagley, P. 1987. Revised 40 Ar/39Ar age for granites of the Mourne Mountains, Ireland. *Scottish Journal of Geology*, **23**, 215–220, <https://doi.org/10.1144/sjg23020215>
- Walker, G.P.L. 1975. A new concept of the evolution of the British Tertiary intrusive centres. *Journal of the Geological Society*, **131**, 121–141, <https://doi.org/10.1144/gsjgs.131.2.0121>
- Wall, F., Rollat, A. and Pell, R.S. 2017. Responsible Sourcing of Critical Metals. *Elements*, **13**, 313–318, <https://doi.org/10.2138/gselements.13.5.313>
- Wall, F., Niku-Paavola, V.N., Storey, C., Müller, A. and Jeffries, T. 2008. Xenotime (Y) from carbonatite dykes at Lofdal, Namibia: Unusually low LREE:HREE ratio in carbonatite, and the first dating of xenotime overgrowths on zircon. *Canadian Mineralogist*, **46**, 861–877, <https://doi.org/10.3749/canmin.46.4.861>
- Walters, A.S., Goodenough, K.M., Hughes, H.S.R., Roberts, N.M.W., Gunn, A.G., Rushton, J. and Lacinska, A. 2013. Enrichment of Rare Earth Elements during magmatic and post-magmatic processes: a case study from the Loch Loyal Syenite Complex, northern Scotland. *Contributions to Mineralogy and Petrology*, **166**, 1177–1202, <https://doi.org/10.1007/s00410-013-0916-z>
- Warner, R., Moles, N. and Chapman, R. 2010. Evidence for early bronze age tin and gold extraction in the Mourne Mountains, County Down. *Journal of the Mining Heritage Trust of Ireland*, **10**, 29–36.
- Whitworth, M.P. and Feely, M. 2011. The geochemistry of selected pegmatites and their host granites from the Galway Granite, Western Ireland. *Irish Journal of Earth Sciences*, **10**, 89–97, <http://www.jstor.org/stable/30002251>
- Wilkinson, C.M., Ganerod, M., Hendriks, B.W.H. and Eide, E.A. 2017. Compilation and appraisal of geochronological data from the North Atlantic

- Igneous Province (NAIP). *Geological Society of London Special Publications*, **447**, 69–103, <https://doi.org/10.1144/SP447.10>
- Williams-Jones, A.E., Migdisov, A.A. and Samson, I.M. 2012. Hydrothermal mobilisation of the rare earth elements—a tale of ‘ceria’ and ‘yttria’. *Elements*, **8**, 355–360, <https://doi.org/10.2113/gselements.8.5.355>
- Wilson, K.R. 2004. The last glaciation in the Western Mourne Mountains, Northern Ireland. *Scottish Geographical Journal*, **120**, 199–210, <https://doi.org/10.1080/00369220418737203>
- Young, M. 2016. The Tellus geoscience surveys of the north of Ireland: context, delivery and impacts. In: Young, M. (ed.) *Unearthed: Impacts of the Tellus Surveys of the North of Ireland*, 3–10, <https://doi.org/10.2307/j.ctt1g69w6r.6>
- Young, M., Knights, K., Smyth, D., Scanlon, R. and Gallagher, V. 2016. The Tellus geochemical surveys, results and applications. In: Young, M. (ed.) *Unearthed: Impacts of the Tellus Surveys of the North of Ireland*, Royal Irish Academy, Dublin, 33–52, <https://doi.org/10.2307/j.ctt1g69w6r.8>
- Yu, C., Drake, H., Mathurin, F.A. and Åström, M.E. 2017. Cerium sequestration and accumulation in fractured crystalline bedrock: the role of Mn-Fe (hydr-) oxides and clay minerals. *Geochimica et Cosmochimica Acta*, **199**, 370–389, <https://doi.org/10.1016/j.gca.2016.11.044>
- Zhao, P., Zajacz, Z., Tsay, A. and Yuan, S. 2022. Magmatic-hydrothermal tin deposits form in response to efficient tin extraction upon magma degassing. *Geochimica et Cosmochimica Acta*, **316**, 331–346, <https://doi.org/10.1016/j.gca.2021.09.011>